

The Meteorological Magazine

November 1993

Local climatological model

Wind shear at cold fronts

Severe hailstorm in Greece

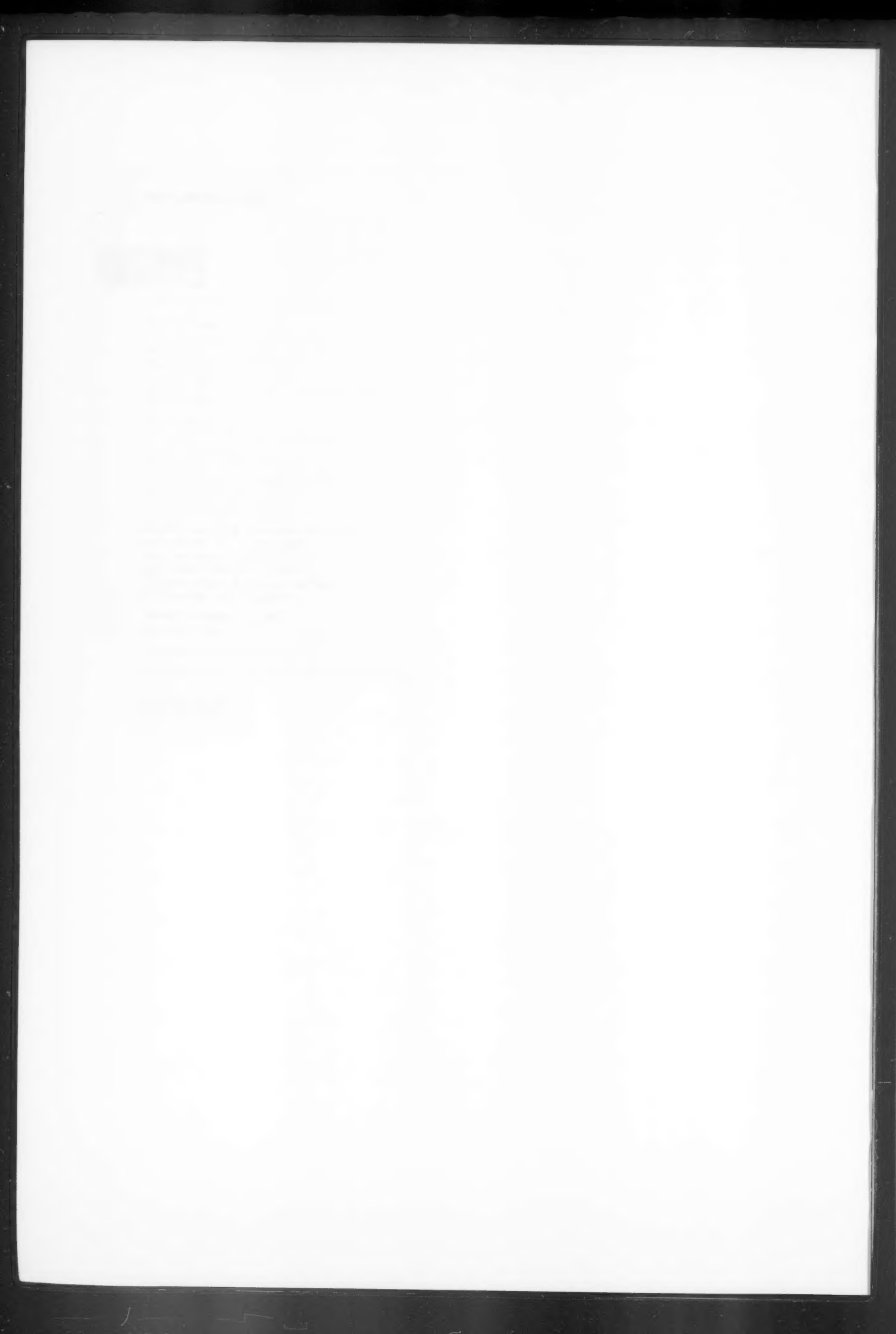
Polar lows over Atlantic

Infrared imagery showing upper-level waves

Use of Willmott's index

Thunderstorm forecasts using thermodynamic indices

Met.O.1010 Vol. 122 No. 1456



The Meteorological Magazine

November 1993
Vol. 122 No. 1456

551.581.1(485):551.509.313.5

Evaluation of a local climatological model — test carried out in the county of Halland, Sweden

T. Gustavsson and J. Bogren

Laboratory of Climatology, Department of Physical Geography, University of Gothenburg, Reutersgatan 2c, S-413 20 Gothenburg, Sweden

Summary

The present paper deals with an evaluation of the Local Climatological Model (LCM) developed at the Department of Physical Geography, University of Gothenburg. The control measurements included in the report are mainly focused upon three different parts in the LCM: (i) variation in road surface temperature under both clear day conditions, and synoptic conditions characterized by cloudy, windy, (ii) control functions in the LCM and (iii) test regarding the possibility of predicting temperature development along stretches of road.

1. Introduction

The local climatological model (LCM) which has been developed at the Department of Physical Geography, University of Gothenburg, is used for calculation of air and road surface temperatures. This paper is a part of a series of reports dealing with modelling of local climate and the extrapolation of temperatures from measuring stations to be valid for larger areas. Previous publications consist of, for example, Bogren (1991), Bogren and Gustavsson (1991a, b), Gustavsson and Bogren (1991a, b), Gustavsson (1990a, b).

The idea behind a road surveillance system is that stations measuring temperatures, humidity and wind should be located in such areas that an early warning of road icing can be achieved. This requires that the stations have various types of locations as different weather situations result in a different temperature patterns.

The background idea behind the LCM is that information about temperature variations along a stretch of road in a given area could lead to a more efficient surveillance of the winter roads. If the decision about

salting action is based upon more diversified information, compared to that received only from the locations of the field stations, the right decision is made more easily. The road attendant can, for instance, decide whether an action needs to be taken or not, and give priority to certain stretches as well.

If a LCM is to be used to give additional information, it is of the greatest importance that the data presented are correct and relevant. Because of this, control measurements were carried out in an area where the model has been adapted. The study presented in this paper was carried out in the county of Halland, in the south-western part of Sweden, and it is focused upon control measurements along specific stretches of road as well as validation of the formulae used in the LCM. This is the second report dealing with this subject. The first (Bogren and Gustavsson 1991b) was mainly concerned with temperature distribution during clear nights and the variation caused by the local topography. Some preliminary studies were also carried out in order to

verify the temperature pattern under other types of weather conditions.

The importance of topography on the variation of air and road surface temperatures has also been studied by, for example, Tabony (1985) and McLean and Wood (1992). The effect of different weather conditions on the temperature pattern has been discussed by Thornes (1989).

Prediction of road surface conditions is made by use of numerical road ice prediction models, e.g. Rayer (1987), Thornes and Shao (1991). The results of such models are used to give information about the forthcoming temperature development at a specific site.

The control measurements presented in this report were conducted by the use of instruments attached to specially designed cars and from analyses of recordings from stations in the Road Weather Information System (RWIS). The study is mainly focused upon the following parts:

- (i) the temperature pattern during clear days, and the difference in road surface temperature (RST) due to the varying intensity of solar radiation;
- (ii) road surface temperature variations during cloudy, windy conditions and especially the control functions in the LCM related to this specific part;
- (iii) the development of temperature patterns during nights with falling temperatures, both regarding the cooling rate for different areas and also the division of the road into smaller segments and;
- (iv) the variation of temperature patterns during periods with a change in temperature.

2. Principles behind the local climatological model

To be able to calculate the temperature pattern along roads using the LCM, several factors need to be considered. For an adaptation of the LCM to a specific area the following data is used.

Thermal mapping: Basic background information is received from thermal mapping of the road net in the county in question under different weather conditions. The results from thermal mapping give valuable information about magnitude and frequency of RST variations along the road caused by different topographical features.

Topographical maps/field studies: From topographical maps and field measurements, information about topography and geographical aspects is considered together with the temperature information from the thermal mapping.

RWIS: Information from the RWIS field stations gives the possibility of considering historical recordings to confirm the temperature variations determined from the thermal mapping.

The integration of these factors results in a classification and separation of different segments along the stretches of road. The most important topographical

segments are: valleys, screened areas, variations in altitude and bridges. Proximity to water and regional climate are also taken into account when a certain area is considered. These fundamental topoclimatological parameters, which must be known in order to calculate temperature variations along a stretch of road, have been described in previous papers (Bogren and Gustavsson 1986; Bogren *et al.* 1992; Gustavsson *et al.* 1987; Bogren 1990; Gustavsson 1990).

When the basic background information is adopted into the model it is possible to start the calculation and extrapolation of the temperature pattern. This process can be divided into three parts. Firstly, the variables measured at the RWIS are collected and stored for 6 hours so that trends can be calculated. Secondly, the algorithm in the model compares air and road surface temperatures for determining the 'type' of temperature variations currently existing in the area in question. The temperature situations included are day/clear, night/clear, cloudy/windy and regional pattern. Thirdly, the model uses empirical formulae to calculate which temperature values should be valid for the segments along the road.

The county of Halland, in which the model has been implemented, was divided into three parts, North, Middle and South. The areas overlap each other to give efficient coverage. Each part has its own reference stations to fulfil the required demands about small topographical influence and a high degree of exposure.

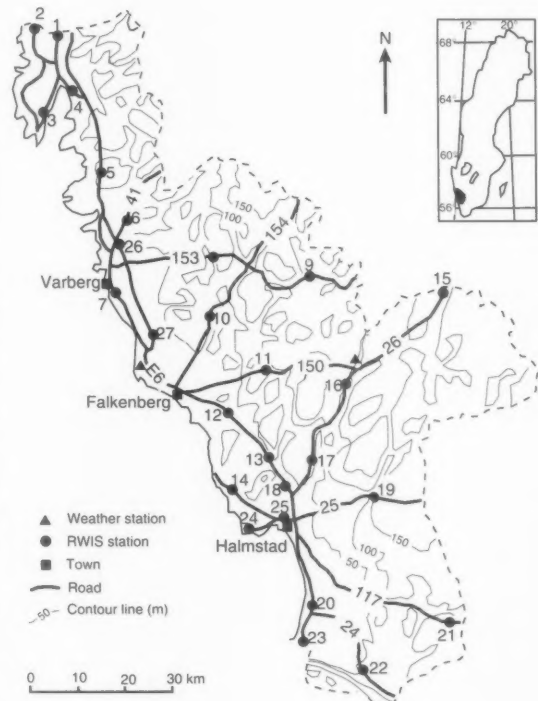


Figure 1. Map of the study area; the county of Halland.

3. Study area

The county of Halland is situated in the south-western part of Sweden between latitudes 56° and 58° N. In this area, 27 RWIS stations are used for the surveillance of winter road conditions. The stations are located along the main roads in the county as shown in Fig. 1. Halland is characterized by a varying topography. In the western part, the coastal zone is flat, mainly arable land. To the east, the open country is succeeded by a hilly, forested landscape. The climate in south-western Sweden is to a high degree determined by the west wind regime. This means that, especially during the winter period, the frequency of low pressure passages is very high. The regional climate is to a large extent influenced by the nearness of the sea. Another significant factor is the change in altitude which occurs approximately 10 to 15 km from the coast. The difference in height between the coastal zone and inland is more than 200 m in some parts.

The coastal zone is often affected by strong winds; further inland, the increasing relief reduces their strength. The precipitation pattern is characterized by a successive increase towards the eastern parts where the elevation increases. Another phenomenon which is important during ice-free winters is that the warm sea can generate a tongue of relatively warm air which reaches inland.

4. Test of the models

4.1 Day/Clear

The effect of screening as a factor causing large road surface temperature variations is connected to clear day conditions. The largest influence of screening, which can affect the risk of slipperiness, occurs during late autumn and early spring. Depending on such factors as orientation, extension and composition of the object causing a shadow pattern in combination with the position of the sun, the magnitude of the temperature differences between sun-exposed and shaded areas varies. Empirical studies using the abundant information supplied by the RWIS and thermal mapping show that it is possible to calculate the screening effect by knowing the orientation of the object and the solar elevation.

The variation in temperature difference between screened and sun-exposed sites, and how the temperature varies according to the time of year is clearly seen when comparing the magnitude of the difference between sun exposed and screened areas at different times of the year. The detail of the two thermal mapping on 5 February and 30 March, respectively, in Fig. 3 illustrates this effect.

This indicates that the greater the amount of incoming solar radiation, the greater the potential for a pronounced screening effect. Assuming this regularity between solar elevation and temperature deficit at screened locations, it is possible to use the solar elevation as a predictor of the road surface temperature difference between sun exposed and screened areas.

The maximum road surface temperature difference between screened and sun-exposed stretches can be

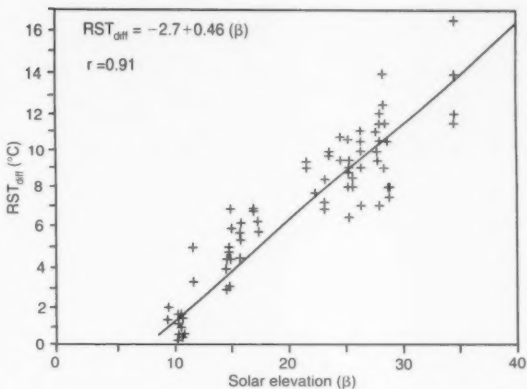


Figure 2. Maximum road surface temperature difference between sun exposed and screened areas as a function of solar elevation.

predicted according to the solar elevation. The relation between solar elevation and RST_{diff} is expressed by the equation,

$$RST_{diff} = -2.7 + 0.46(\beta) \quad (1)$$

where β is the solar elevation in degrees

Using the relation expressed by equation (1) it is seen that during December/January when the midday sun is lowest at approximately 10° above the horizon, the temperature difference is very small, just 2 °C. At the end of March, when β is 35°, the difference increases to more than 13 °C, Fig. 2. These calculated temperature differences are in good agreement with those shown by Fig. 3.

In the model, the variation in the solar elevation throughout the season is calculated. The progress of the increasing solar elevation at noon changes according to a non-linear relation throughout the year. The change of the daily variation in solar elevation is given by

$$\sin\beta = \sin\phi \sin\delta + \cos\phi \cos\delta \cosh h \quad (2)$$

where ϕ is the latitude of the site, δ is the solar declination and h is the hour angle.

The declination (δ) as a function of the day of the year (N) is given by

$$\delta = -23.4 \cos(360(N+10)/365). \quad (3)$$

The maximum solar elevation at noon is calculated using $\beta = (90^\circ - \phi) + \delta$.

For practical use, when adopting the local climatological model, it is necessary to distinguish six different types of screening situations to observe this effect along a road: S0 — sun exposed, S1 — screened during the morning hours, S2 — screened at noon, S3 — screened in the afternoon, S4—S1 and S2 in combination, S5—S2 and S3 in combination, S6—S1 and S3 in combination.

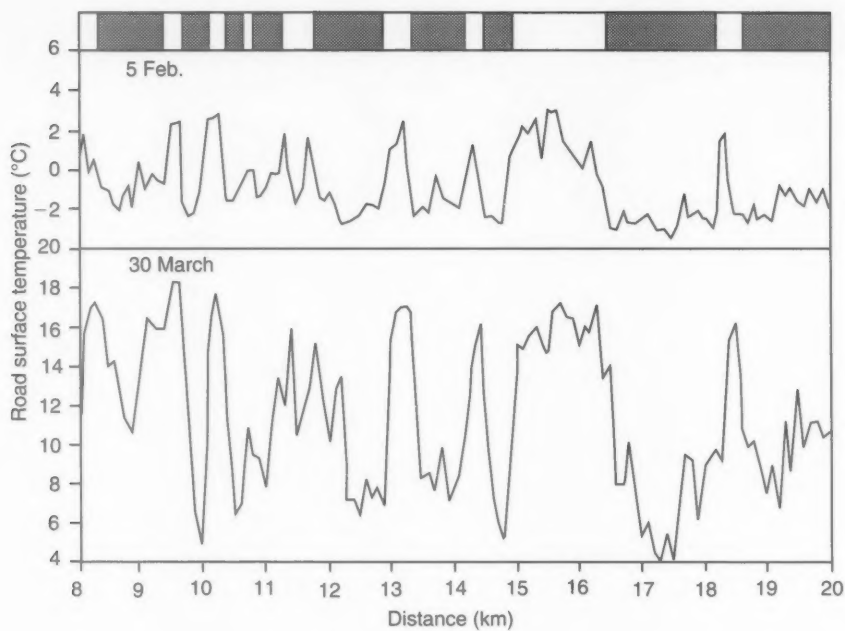


Figure 3. Detail of thermal mapping along road No. 25, from 5 February and 30 March, 1992. The screened areas are marked on the top of the figure.

Large areas of Halland are affected by screening. However, most of the screening effect is caused by dense coniferous forest and, in some cases, the screening effect is strengthened by local topography. Screening by road rock cuts occurs in only a few places.

A good example of how the RST can vary along a road as a result of alternating screened and sun-exposed areas is given by the detail from thermal mapping in Fig. 3. The two sections are from thermal mapping carried out just after noon along road No. 25 east of Halmstad on 5 February and 30 March, respectively.

Three main features regarding the effect of screening on the RST are obvious. Firstly, that the drop in temperature associated to the screened section occurs very distinctly within a short distance and, secondly, the shadow pattern is kept throughout the season. Thirdly, the difference between sun exposed and screened areas grows according to the established relation with the increasing solar elevation.

If clear/day conditions should be valid, the recorded RST_{diff} between reference stations and screened stations must fulfil the requirements which are stipulated by the algorithm in the LCM. The limits for the formulae, which determine whether there is a screening effect or not, are adjusted according to the time of the year and time of the day to allow for variations in solar elevation.

4.1.1 Control measurements

The test of the day/clear temperature pattern was performed for the roads in Halland. Regarding the screening effect, the results from road Nos. 150, 26 and 25 are presented in Tables I, II and III. The roads were

thermally mapped during three different periods, 5 February, 4 March and 30 March 1992. The control measurements were carried out during the forenoon and at noon. The results from these measurements (meas) are compared to the calculated values (calc). The weather conditions in these situations are characterized by clear sky and moderate winds.

The result from the day/clear situations shows that the segmentation matches well with the temperature pattern which is generated by the alternation between screened and sun exposed. Comparing the calculated RST_{calc} and the measured RST_{meas} it is seen that the differences vary depending on the time of day and the time of year when the control measurements are performed.

The best correlation between calculated and measured is found close to noon. This can be explained by the orientation of the roads which favours distinct shadow patterns during the midday hours. There is also a tendency towards an increased error when the solar elevation is very high late in the season. During this period the slope of the sun-exposed road has a great influence on the insolation which makes the RST of the sun-exposed parts vary. When the sun-exposed areas (S0) get temperatures in the range well above +10 °C the accuracy of the calculated temperature is somewhat worse. It should be pointed out that the accuracy of the temperature calculation of the S0 segments is of no importance when the model is in use for winter road surveillance. However, when testing the day/clear temperature pattern, it is found that the difference between calculated and measured values is generally less than 1.0 °C throughout the season. An important result is

Table I. Comparison between measured and calculated road surface temperatures along road No. 150 for clear day conditions.

Segment No.	Distance (km)	Type	5 Feb.			4 March			30 March		
			Calc	Meas	Diff	Calc	Meas	Diff	Calc	Meas	Diff
1	00-12	S0	3.3	3.0	0.3	12.5	12.0	0.5	17.3	17.5	0.2
2	12-15	S1	-1.9	-2.2	0.3	12.5	13.0	0.5	17.3	17.0	0.3
3	15-18	S2	-1.9	-3.0	1.1	6.6	4.0	2.6	4.0	6.0	2.0
4	18-19	S3	3.3	3.0	0.3	4.0	4.0	0.0	4.0	6.0	2.0
5	19-36	S1	-1.9	-3.0	1.1	12.5	12.0	0.5	17.3	17.0	0.3

Table II. Comparison between measured and calculated road surface temperatures along road No. 26 for clear day conditions.

Segment No.	Distance (km)	Type	5 Feb.			4 March			30 March		
			Calc	Meas	Diff	Calc	Meas	Diff	Calc	Meas	Diff
1	00-05	S0	1.8	1.0	0.8	12.6	12.0	0.6	7.5	10.0	2.5
2	05-10	S6	-2.4	-1.5	0.9	6.8	4.0	2.8	-0.1	2.0	2.1
3	10-12	S0	1.8	1.0	0.8	12.6	12.0	0.6	7.5	10.0	2.5
4	12-13	S6	-2.4	-1.5	0.9	12.6	12.5	0.1	-0.1	2.0	2.1
5	13-16	S0	1.8	1.0	0.8	12.6	13.0	0.4	7.5	10.0	2.5
6	16-25	S1	-2.4	-2.8	0.4	12.6	12.0	0.6	0.1	2.0	1.9
7	25-29	S0	1.8	1.0	0.8	12.6	13.0	0.4	7.5	10.0	2.5
8	29-39	S4	-2.4	-2.5	0.1	6.6	4.0	2.8	0.1	2.0	1.9

Table III. As Tables I and II but for road No. 25.

Segment No.	Distance (km)	Type	5 Feb.			4 March			30 March		
			Calc	Meas	Diff	Calc	Meas	Diff	Calc	Meas	Diff
1	00-10	S0	3.5	4.0	0.5	14.5	13.0	1.5	16.8	18.0	1.2
2	10-11	S2	-1.7	-2.0	0.3	8.2	7.0	1.2	3.4	4.5	1.1
3	11-12	S0	3.5	4.0	0.5	14.5	13.0	1.5	16.8	18.0	1.2
4	12-15	S1	3.5	4.0	0.5	14.5	13.0	1.5	16.8	18.0	1.2
5	15-16	S0	3.5	4.0	0.5	14.5	13.5	1.0	16.8	17.5	0.7
6	16-17	S1	3.5	4.0	0.5	14.5	13.0	1.5	16.8	17.0	0.2
7	17-19	S5	-1.7	-2.0	0.3	8.2	7.0	1.2	3.4	4.0	0.6
8	19-27	S0	3.5	4.0	0.5	14.5	13.5	1.0	16.8	18.0	1.2

that calculations of the RST at the screened segments (S1-S6) give good agreement with the measured values.

4.2 Cloudy/windy

Depending on the temperature change with height, the atmosphere can be classified as unstable, neutral or stable. If the atmosphere is neutral the temperature lapse rate is equal to $1\text{ }^{\circ}\text{C}/100\text{ m}$; in an unstable atmosphere the temperature change with height is larger and the opposite is the case for a stable atmosphere. Factors with an influence on the vertical temperature gradient are the wind and the amount of cloud.

A relationship between the meteorological conditions and the type of stability was presented by Pasquill (1961) (Table IV). This type of relationship is widely used in connection with calculations of concentrations of air pollution. However, this knowledge can also be used in the LCM as a base for decisions concerning the type of temperature formulae that should be used.

Under daytime conditions, insolation is a most important parameter. Several studies have demonstrated

Table IV. Meteorological conditions defining stability types according to Pasquill (1961).

Surface wind (m s ⁻¹)	Daytime insolation			Night-time	
	Strong	Moderate	Slight	Thin overcast or >1/4 low cloud	Cloud <1/4
<2	A	A-B	B	E	F
2-3	A-B	B	C	E	F
3-4	B	B-C	C	D	E
4-6	C	C-D	D	D	D
6	C	D	D	D	D

A = Extremely unstable; B = Moderately unstable; C = Slightly unstable; D = Neutral; E = Slightly stable; F = Moderately stable.

a close relationship between type of clouds and rate of insolation, e.g. Nielsen *et al.* (1981). However, the road surface temperature is affected in a somewhat different way compared with the air temperature. Studies by

Bogren (1991) and Gustavsson and Bogren (1991) have shown that large variations in RST can exist despite the fact that the difference in air temperature is very small. The result is that the model uses the formulae for clear day conditions for all wind speed classes listed in Table IV. The variation owing to decreased insolation/increased amount of clouds is dealt with from comparison of the temperature differences between reference locations, i.e. in sun-exposed areas, and screened locations.

Under night-time conditions, a clearer distinction exists between the different types of formulae to be used in the model. If the cloudiness is less than 3 oktas and the wind speed is below 5 m s^{-1} the model uses the algorithm for clear night-time conditions. This part of the model further includes a division made owing to the prevailing wind speed during the latest 3 hours, determined from RWIS stations with wind-speed sensors.

The regional pattern is used in the LCM if the criteria for temperature decrease with height is not fully achieved or if the temperature pattern is too complex to be classified as belonging to any of the other types. In the case of regional pattern, the local RWIS station is used as a base for the extrapolation of the temperatures to be valid for parts of road.

The conclusion that can be drawn from Table IV is, however, that the formulae used for neutral and unstable conditions are several. Especially with a relatively high wind speed and reduced insolation during the day, or reduced cooling during the night, the criteria for the conditions related to 'variation in altitude' are normally fulfilled. Another important matter is that cloudy, windy weather situations are very frequent in southern Sweden which makes this part of the model a most important subject to study in more details.

The temperature lapse rate can be determined from temperature measurements on towers, masts, etc. However, RWIS stations sited on different altitudes can also be used to determine the lapse rate. Several stations must be included in the calculation and it is also important that the formula is limited to a relatively small area as local variations in the weather can have a large effect on the temperature.

In the model, the correlation coefficient is used as a control for the calculations. The correlation between temperature and variation in altitude must be high for the model to calculate the temperature for stretches of roads according to this division. Furthermore, a division is made according to the calculated lapse rate, i.e. the lapse rate must be greater than a fixed value if the model should use this part.

As previously mentioned, the amount of cloud and the prevailing wind speed are most important factors determining the temperature lapse rate. The following example shows the development from a scattered temperature pattern (regional pattern in the LCM) to a fully mixed atmosphere — neutral and later unstable air

stratification. The stations in the northern part are used to illustrate the development, as well as the temperature pattern revealed by the recorded road surface temperature at the RWIS stations. In total, 8 stations were used for the calculation of the temperature lapse rate and the correlation coefficient for the time period 0200 to 1600 hours, Figs 4 and 5. The wind speed recorded for the same time period at station 7 is shown in Fig. 6.

The meteorological conditions during this episode (1 to 2 December 1990) were characterized by a change in the weather. During the evening of 1 December, the sky was clear and a light wind was blowing, i.e. large temperature contrasts developed owing to the local

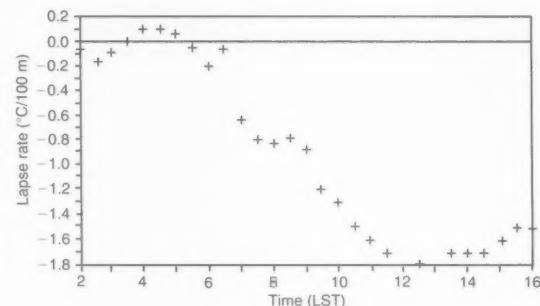


Figure 4. Plot of calculated temperature lapse rate for the northern stations in Halland, 2 December 1990.

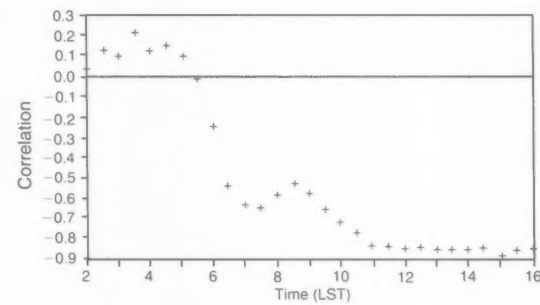


Figure 5. The correlation between height and road surface temperature for 2 December 1990.

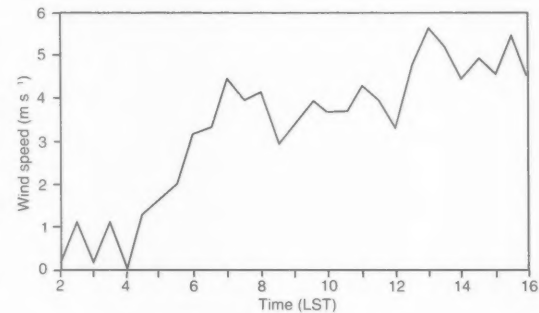


Figure 6. Wind speed recorded at station 7 for 2 December, 1990.

climatological environment and other factors near the different station sites. A front reached the western part of Sweden early the following morning. The wind speed increased from $1-2 \text{ m s}^{-1}$ to $4-6 \text{ m s}^{-1}$ and the amount of cloud changed from no cloud to overcast conditions. The calculated temperature lapse rate shows that, during the first hours of the weather change, the temperature variations are not related to the variation in altitude. This is further confirmed by the correlation coefficient between height and RST. During periods with low correlation and a complex temperature distribution, the model uses the regional pattern for calculation of the variation along stretches of road. As the correlation increases and the lapse rate indicates a temperature decrease with height, the model chooses the part of the LCM dealing with variation in altitude. From comparison of the data presented in Figs 4, 5 and 6 it is obvious that a close relation exists between the factors. A relatively high wind speed leads to a mixed atmosphere, and as the lapse rate increases the correlation increases as well.

4.2.1 Control measurements

Several temperature measurements have been carried out under cloudy, windy conditions, and the roads from the coastline towards the county border in the east were specially chosen for study; they were chosen because a rather large change in altitude occurs here.

A height profile for road No. 25 is shown in Fig. 7 together with a recording of the RST during 26 February

1992 at 1900 h (Fig. 8). The measurement started outside of Halmstad, at 20 m above sea level and ended at the county border at a height of approximately 150 m AMSL. A distinct change in altitude occurs at 16 to 18 km from the starting point.

The difference in road surface temperature is equal to $1 \text{ }^{\circ}\text{C}$, a drop from 3.8 to $2.8 \text{ }^{\circ}\text{C}$. However, the drop in RST is not only controlled by the regional variations in altitude, other small variations have an effect on the temperature distribution.

In general, there is a good agreement between height and surface temperature. Additional factors which influence the surface temperature is the relative openness around the road, i.e. the occurrence of trees and woods. Another important factor is the history of the surface temperature. The measurement shown in Fig. 8 was conducted a few hours after a change in cloud amount, and the effect from the weather type preceding the measuring trip also has some influence on the temperature pattern. A calculation of the temperature lapse rate from the RWIS stations in the actual area shows a good agreement with the pattern depicted in Fig. 8. The temperature difference between station 14, sited close to the coastline, and station 19, located close to the county border in the eastern part of the study area, amounts to $0.9 \text{ }^{\circ}\text{C}$. This temperature difference was kept during the night owing to the stable weather situation. From analyses of temperature recordings from the RWIS station in the middle part of the county it is also clearly seen that a change in weather occurred during the day as

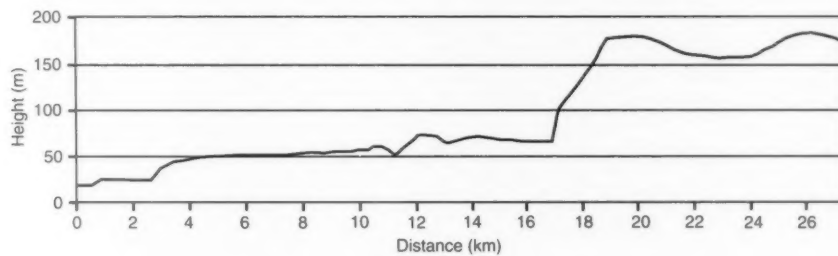


Figure 7. Height profile road for No.25.

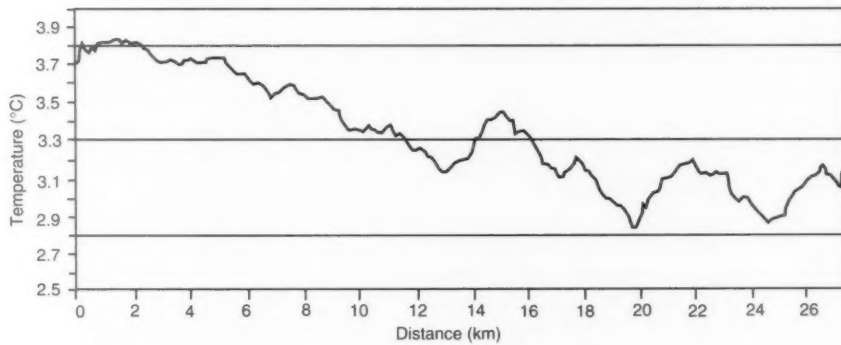


Figure 8. Surface temperature of road No. 25 recorded on the 26 February 1992 at 19:00h.

previously discussed for the measurement along road No. 25.

4.3 Temperature development

Repeated temperature measurements were carried out along the same routes during periods with falling temperature. These measurements have been analysed in order to determine the cooling rate of both the air and the road surface. Temperature recordings from RWIS stations show that the temperature development for the air as well as for the surface differ during the cooling period. The cooling rate (Cr) can be defined as

$$Cr = \frac{dT}{dt} \quad (4)$$

where dT is the change in air or RST over the time period considered (dt).

It is obvious from analyses of recordings from different RWIS stations that the cooling rate is influenced to a large extent by the local climatological factors such as topography, sky-view factor, degree of wind shelter, etc. A study of factors influencing the cooling rate for both the air and surface is presented in Gustavsson (1993). It was shown that, for example, the sky-view factor had a great influence on the development of the surface temperature during clear nights but the effect on the air temperature was very small.

The air temperature pattern along road No. 153 in the northern part of Halland is shown in Fig. 9. The two curves represent measurements carried out at 2100 h (the upper curve) and at 0600 h the following morning. The patterns of the two measurements are very similar and it is clear that the local degree of wind shelter and the local topography had a pronounced effect on the air temperature.

The segments for road No. 153 are also included in Fig. 9 for clear night-time conditions. The resemblance between the temperature pattern and the different segments is most evident. The lowest air temperatures were to be found in the small valleys that the road

crosses and in open wind-sheltered locations in the forested eastern part of the road.

The difference in air temperature between the two measuring trips shows that the cooling rate differs between the segments along the discussed road (Fig. 10). In the figure, the zero values indicate that no change in temperature takes place during the 9 hours which have passed since the first recording was carried out. Negative values show that the area has been relatively colder.

A very important conclusion that can be drawn from the data presented in Figs 9 and 10 is that the relation between the segments developed during the first measuring trip is kept throughout the night. Another important conclusion is that the relative position, the borderlines between the segments, does not change during the cooling period. These two facts are essential to the basis of the model as they show that no alternation of the segments should be made in relation to the length of the cooling period and that the formula linked to each segment could be kept during the night. However, it is important that it is possible to change the relative difference between the segments, i.e. the formulae should not include static correction terms; instead a dynamic correction is required.

The recordings of the RST are shown in Fig. 11 for the same occasion as in Fig. 9. Measurements of the RST with the use of infrared equipment are very sensitive to small variations in the emissivity as well as other factors affecting the surface but not the real temperature. In order to exclude RST values which do not represent the true temperatures, the average temperature values have been used in the analyses. Running means of 10 values were used in the calculation and these are the data presented in Fig. 11.

The temperature distribution along road No. 153 is very similar for both measuring trips. The resemblance between the pattern in Figs 9 and 11 (air and RST) is also clearly seen, i.e. there is a close correlation between segments with a low air and road surface temperature.

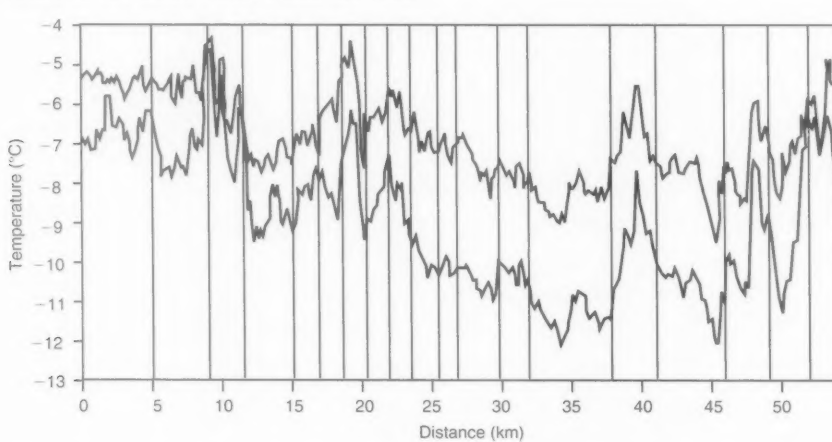


Figure 9. Air temperature pattern along road No. 153 at 2100 h and at 0600 h. The vertical lines mark the different segments along the road.

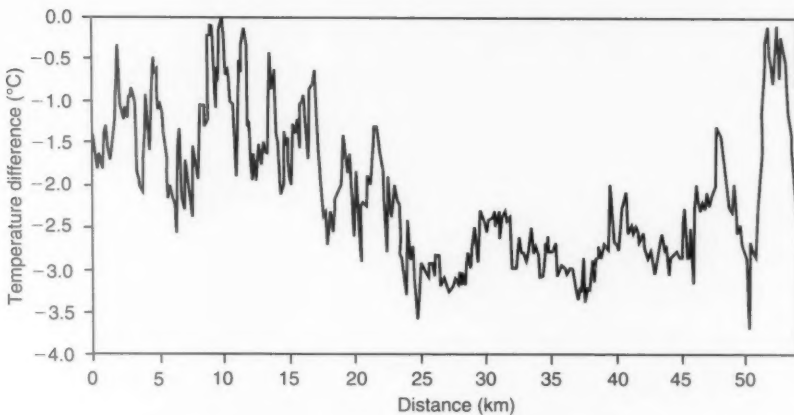


Figure 10. Difference in cooling rate between segments along road No. 153. The zero value indicate that no change in temperature takes place.

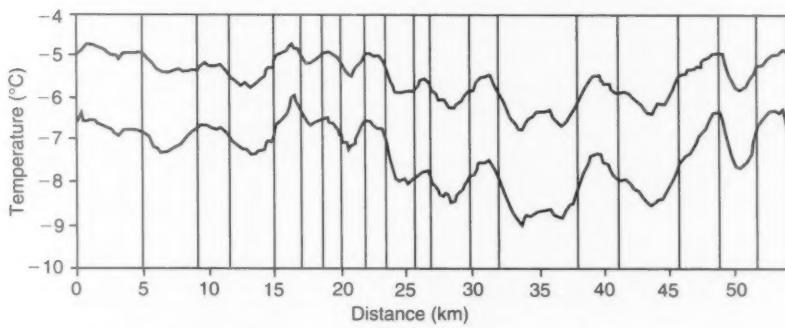


Figure 11. Recording of road surface temperature along road No. 153, see also Fig. 10.

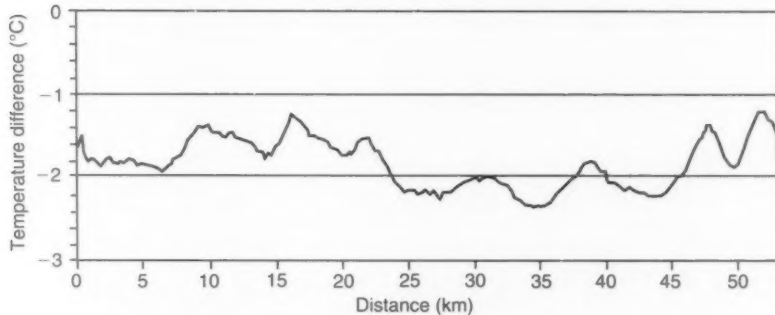


Figure 12. Difference in road surface temperature between measurements at 2100 h and 0600 h respectively.

As for the air temperature, the difference in RST was calculated between the two measuring trips, Fig. 12. It is clearly seen that the cooling rate differs between the segments which is in good agreement with the result shown for the air temperature. The mean values for each segment were used to calculate the change in temperature from 2100 h to 0600 h as well as the resulting cooling rate for each area, Table V.

The cooling rate varies from 0.15 to $0.28 \text{ }^{\circ}\text{C h}^{-1}$. The largest cooling rate is associated with the area which has the lowest temperature during both measurements. This indicates that the contrast in surface temperature becomes larger with a longer cooling period. The areas with the smallest Cr value are small hills and areas with trees close to the road side. These two factors both lead to a reduced cooling. On hills, the accumulation of cold

Table V. Calculated cooling rate for the measurements along road No. 15 and the relative difference in temperature between the segments.

Segment	Temp. (°C)	Diff.* (°C)	Temp. (°C)	Diff.* (°C)	Cooling rate (°C h ⁻¹)
1	-4.9	0.1	-6.7	0.5	0.2
2	-5.4	0.6	-7.3	1.1	0.2
3	-5.3	0.5	-6.7	0.5	0.15
4	-5.6	0.5	-6.7	0.5	0.19
5	-4.8	0.0	-6.2	0.0	0.2
6	-5.2	0.4	-6.6	0.4	0.15
7	-4.9	0.1	-6.4	0.2	0.17
8	-5.4	0.6	-7.2	1.0	0.2
9	-5.0	0.2	-6.6	0.4	0.18
10	-5.8	1.0	-8.0	1.8	0.24
11	-5.5	0.7	-7.8	1.6	0.25
12	-6.2	1.4	-8.4	2.2	0.24
13	-5.5	0.7	-7.5	1.3	0.22
14	-6.4	1.6	-8.9	2.7	0.28
15	-5.5	0.7	-7.5	1.3	0.22
16	-6.3	1.5	-8.5	2.3	0.24
17	-5.2	0.4	-6.5	0.3	0.14
18	-5.8	1.0	-7.5	1.3	0.19
19	-5.2	0.4	-6.5	0.3	0.14

*Diff = Difference in RST versus segment No.5

air is prevented and trees close to the road side obstruct cooling by radiation.

The relative temperature differences along the road are also included in Table V. This difference was determined in relation to the warmest segment, No. 5, on both occasions. During the first trip, the maximum difference amounted to 1.6 °C but the average value is less than one degree. The relative difference in RST increased during the second trip compared with the recording carried out during the evening. The maximum difference was 2.7 °C and several segments were more than 1 °C colder.

The knowledge obtained from this analysis is essential making a temperature prognosis with the use of the LCM. However, the integration of an external prognosis, and the corrections that must be made in the model, are subjects which need to be studied further before such a function could be included in the Local Climatological Model.

5. Discussion

Tests of the local climatological model which were performed in Halland show that by use of such a model it is possible to increase the information available from the RWIS. The local climatological model gives the advantage of temperature information for entire stretches of road based on the measurements at the RWIS stations together with the different topographical segments along the roads.

When implementing the model into a new area, it is necessary to have access to high-quality thermal mapping in order to segment the road. Thermal mapping

must also be available for all the different weather conditions which are included in the model. Results from thermal mapping also serve as a complement to the historical RWIS data when the different formulae are determined for the different segments and limits for the varying weather conditions are established.

The results of the different tests reported in this study show that calculated temperatures along the stretches of road are in good agreement with control measurements. The evaluation shows that the design of the criteria which are used at present are well suited to separate the thermal pattern at the main weather categories which are used today. In the discussion of how well the measured values fit the calculated values it is important to include the question of the spatial resolution demanded.

The formulae which are used for the calculation of the temperature pattern allows a higher resolution on the temperature calculation than is needed. For practical purposes one must limit the length of the different segments on the different occasions to not less than 500 m. A higher resolution is not applicable when a dense network is surveyed. This means that the average conditions within the segment must be established.

However, it is necessary to develop the functions to take all possible temperature patterns into account. A possible way of developing the control criteria would be to include a comparison with historical temperature distributions, i.e. a comparison with statistically verified temperature patterns is made in the LCM before the data is extrapolated to be valid for stretches of road.

Further work with the model will include an addition of a road surface temperature prognosis to the present model. To make a prognosis have good validity, it is important to include some sort of external forecast giving information of, for example, cloudiness. It is especially important to study further the variation in such factors as cooling rate to be able to determine the difference in temperature development for the segments along roads which must be used in connection with the temperature forecast which is given for the specific RWIS station.

Acknowledgments

The tests in this project were financially sponsored by Test Site West Sweden — ARENA. The main project is sponsored by the Swedish National Road Administration.

References

- Bogren, J., 1990: Application of a local climatological model for prediction of air and road surface temperatures. Department of Physical Geography Gothenburg, GUNI Report 31. (Ph.D Thesis).
- , 1991: Screening effects on road surface temperature and road slipperiness. *Theo Appl Climatol.* **43**, 91–99.
- Bogren, J. and Gustavsson, T., 1986: A method for the development of a local climatological model for prediction of slipperiness on roads. Department of Physical Geography Gothenburg, GUNI Report 20.
- , 1991a: Nocturnal air and road surface temperature variations in complex terrain. *Int J of Climatol.* **11**, 443–455.
- , 1991b: Strackanpassad klimatmodell. Test site west Sweden.
- Bogren, J. and Gustavsson, T. and Lindqvist, S., 1992: A description of a local climatological model used to predict temperature variations along stretches of road. *Meteorol Mag.* **121**, 157–164.

Gustavsson, T., 1990a: Variation in road surface temperature due to topography and wind. *Theor Appl Climatol*, **41**, 227-236.

—, 1990b: Modelling of local climate with applications to winter road conditions. Department of Physical Geography Gothenburg, GUNI Report 30. (Ph. D Thesis).

—, 1993: A study of air and surface temperature variations during clear windy nights. Submitted to *J Appl Meteorol*.

Gustavsson, T. and Bogren, J., 1991a: Infrared thermography in applied road climatological studies. *Int J Remote Sensing*, **12**, 1811-1828.

—, 1991b: Use of a local climatological model for the prediction of air and road surface temperatures along road stretches. Department of Physical Geography Gothenburg, GUNI Report 29.

Gustavsson, T., Bogren, J. and Lindqvist, S., 1987: Seminar in road weather climatology — Oct. 1987. Department of Physical geography, GUNI Report 25.

McLean, P.J. and Wood, N.L.H., 1992: Coastal influence on winter road surface temperatures in the county of Devon. United Kingdom.

Third Int. Symposium on Snow Removal and Ice Control Technology. September 14-18, 1992. Minneapolis, Minnesota, USA.

Nielsen, L.B., Prahm, L.P., Berkowicz, R., and Conradsen, K., 1981: Net incoming radiation estimated from hourly global radiation and/or cloud observations. *J Climatol*, **1**, 255-272.

Pasquill, F., 1961: The estimation of the dispersion of wind-borne material. *Meteorol Mag*, **90**, 33.

Rayner, P.J., 1987: The Meteorological Office forecast road surface temperature model. *Meteorol Mag*, **116**, 180-191.

Tabony, R.C., 1985: Relations between minimum temperature and topography in Great Britain. *J Climatol*, **5**, 503-520.

Thornes, J.E., 1989: A preliminary performance and benefit analysis of the UK national road ice prediction system. *Meteorol Mag*, **118**, 93-99.

Thornes, J.E. and Shao, J., 1991: A comparison of UK road ice prediction models. *Meteorol Mag*, **120**, 55-57.

551.554:551.515.82

Low-level wind shear at cold fronts

C.P. Pelly

Meteorological Office, Larkhill

1. Introduction

This study was made to investigate not only the values of vertical wind shears commonly encountered near to, and ahead of cold fronts, but also their time history and persistence.

A brief survey was also undertaken of some of the extreme values of shear that occur together with their frequency and persistence.

To this end, wherever possible, active cold fronts were considered. Fourteen cases were examined, namely those of 15/3/88, 22/3/89, 10/2/90, 13/3/90, 5/6/90, 21/2/91, 26/2/91, 6/4/91, 26/6/91, 11/7/91, 3/10/91, 19/12/91, 9/5/92 and 16/11/92. Three of these cases (21/1/91, 26/2/91 and 6/4/91) were found to have split-front characteristics.

2. Method

Raw wind data comprising azimuth, elevation and slant range from radiosonde and radar wind soundings are received by Cossor radar and processed to give spot winds; in the case of the Mk. III radiosonde system (1988 to 1990) these were received every 7 seconds and with the Mk. IV system (after 1990) they were received every 2 seconds.

Spot wind values at 150-metre intervals are measured at Larkhill on a routine basis and these were used to calculate the wind shears. To increase the accuracy, a smaller height interval was tried but found to be unsatisfactory as it introduced abnormally high shear values. Crossley (1962) has in fact quoted a source (unpublished) which substantiates such values, the argument being that the smaller the height interval taken

the greater is the trend for the vertical shear to increase excessively to unrealistic values, due to its increased dependency on the local eddy structure.

In order to calculate the times of occurrence of shears above the surface relative to the cold front it was necessary to construct a vertical profile of the front on to a graph having height as the vertical axis and time as the horizontal axis. This was done by plotting a hodograph of the first sounding done in the air mass immediately behind the cold front, in order to establish the height of the frontal surface at this time.

Shears were measured in kn/1000 ft from 1000 to 5000 ft AGL, at 500 ft (150 m) intervals, taking both speed and direction into account. Data below 1000 ft AGL were not used since these values often had to be estimated due to the time taken to lock-on to a radar target. It should also be noted that the vertical shears measured are apparent rather than true values, being the difference between two radar-sensed winds averaged over a layer.

Owing to the limited period each day over which flights were done for operational requirements, it was found that there was a time window of about ten hours (from T-7 to T+3, where T is time of passage of surface cold front) outside of which wind shear data was unobtainable or unreliable.

3. Results

3.1 Mean value

Shears for the fourteen cases were measured and varied from around 3 kn/1000 ft at distances greater than

200 miles from the front and at levels above 2500 ft, to 10 kn/1000 ft near the bottom of the boundary layer. This latter value was taken as a suitable lower limit for the study which follows.

The mean shears are calculated using the highest value found (when this exceeds 10 kn/1000 ft at a specific height). In Table I, column three (No. of cases) refers to the sample size (maximum 14 occasions) used to calculate mean shears.

3.2 Low-level jet

Fig. 1 shows mean start and finishing times of shears ≥ 10 kn/1000 ft, for the fourteen cold front cases and plotted at eight spot heights between 1000 and 5000 ft. Pecked lines are isopleths of shears ≥ 20 kn/1000 ft, i.e. the zone where and when extreme values occur. This higher limit is discussed in section 3.5.

A vital factor in the development of low-level jets is the existence of a tongue of warmer and moister air just ahead of the cold front due to the increased gradient often found within about 60 miles of many cold fronts. One of the effects of this warm, moist tongue is to create a reversal of horizontal temperature gradient fairly close to the cold front (i.e. temperature rising somewhat as the cold front approaches), extending up to around 6000 ft AGL. This has the effect of causing the geostrophic wind to decrease with height, reaching a minimum at or close to the 10 000 ft level near the top of the thermally driven convective layer. A jet maximum is thus created lower down (Browning and Pardoe 1973).

3.3 Persistence

A similar pattern to the time-history figure is evident when a study of the shear persistence scatter diagram (Fig. 2) is made. It is interesting to note the high

incidence of short-lived shears near to and just above the low-level jet core; these shears are probably associated with the maximum jet-core speed.

3.4 Distribution

The relationship between height interval and shear values was discussed briefly in section 2. It was thought pertinent to include some examples of this from the investigation. Two cases were examined and the results are tabulated in Table II. In addition, the relationship between height interval and shear persistence was investigated and, as can be seen below, this gave the reverse effect to shear size, though this only became apparent with the smallest height intervals.

3.5 The frequency and persistence of extreme vertical wind shears with values ≥ 20 kn/1000 ft

Fourteen cases were examined out to an average distance of 300 miles from the cold fronts. In five cases no extreme values were reached in the layer 1000 to 5000 ft AGL. In the remaining nine cases there was a

Table I. Statistics on magnitude of shears > 10 kn/1000 ft

Height	Mean shear	No. of cases	Max. shear
5250	14.0	4	18.0
4750	12.8	8	19.5
4250	11.4	12	15.0
3750	12.6	11	16.0
3250	15.4	10	22.0
2750	14.7	10	20.0
2250	15.0	11	20.0
1750	15.4	13	21.0
1250	16.7	12	28.0

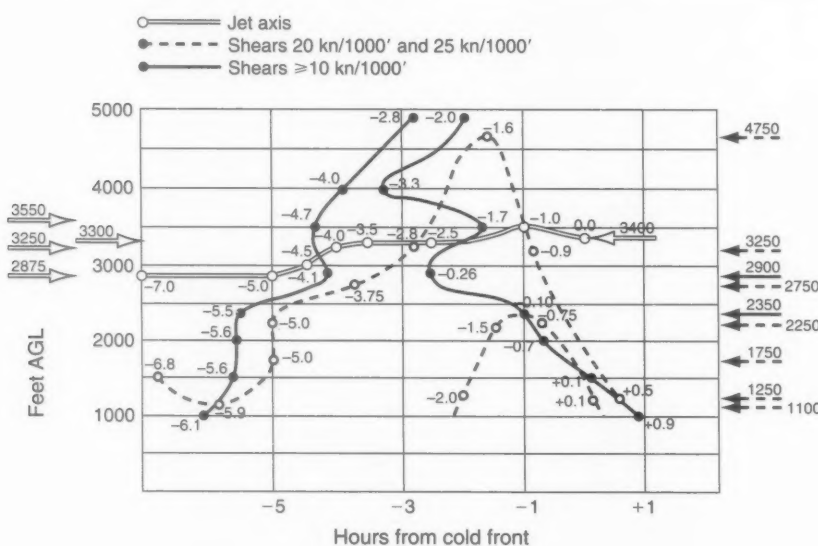


Figure 1. The time-history of shears ≥ 10 kn/1000 ft prior to the passage of ana-cold fronts.

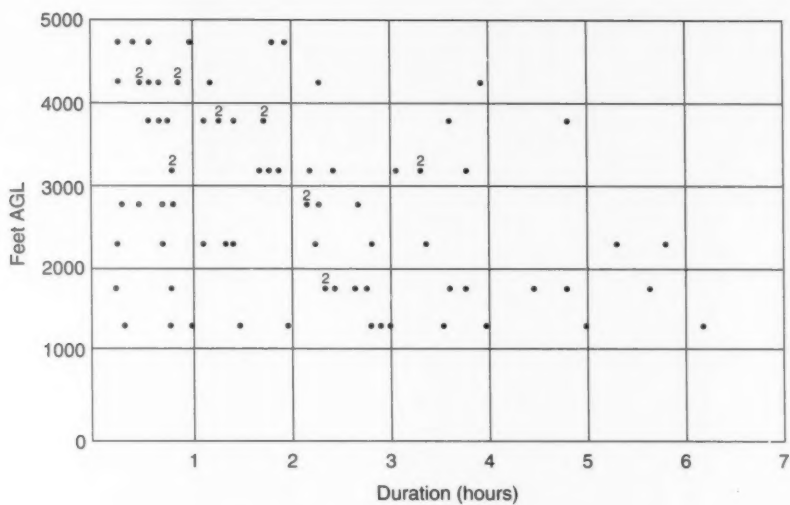


Figure 2. Persistence of shears at different heights.

Table II. Two examples of shear size and persistence (all times UTC)

Shear size in kn/1000 ft on 15 March 1988

Height\Time interval (ft)	0700	0900	1100	1300
1000	3	4.5	7	10
500	5	6	10	12
100	20	16.5	16.5	33

Shear persistence in kn/1000 ft on 15 March 1988

Height\Period interval (ft)	07-09	09-11	11-13	Mean (07-13)
1000	1.5	2.5	3	2.3
500	1	4	2	2.3
100	3.5	0	16.5	6.7

Shear size in kn/1000 ft on 15 March 1988

Height\Time interval (ft)	0700	0900	1100	1300
1000	10	4.5	9.5	5.5
500	11	5	12	14
100	16.5	11	23.5	20.5

Shear persistence in kn/1000 ft on 15 March 1988

Height\Period interval (ft)	07-09	09-11	11-13	Mean (07-13)
1000	5.5	5	4	4.8
500	6	7	2	5
100	5.5	12.5	3	7

remarkably even distribution both temporally and spatially of extreme values.

It was found that those furthest from the cold front had durations varying from 15 to 45 minutes, while those nearer the frontal boundary were a little more persistent lasting from 45 to 90 minutes.

As might be expected from their high values, the frequency of extreme shears was low, in the layer 1000 to 2000 ft where the highest values were most common, extreme shears accounted for only 3.6% of total occasions.

4. Anomalous case history

In the thirteen of the cold front cases considered, the presence of the low-level jet was apparent in varying strengths close to or slightly above the 3000 ft level.

There was, however, one occasion (21 February 1991) when this pre-frontal jet was absent. An examination of the wind profile ahead of the front on this occasion showed only very weak warm advection at all levels to 5000 ft, suggesting an absence of the characteristic tongue of warm air. In view of the drier and somewhat cooler track than usual of the low-level flow (southerly rather than west or south-westerly as in other cases), this conclusion seems reasonable. Also, this particular front was identified as having split front characteristics with much drier air probable above about 6000 ft ahead of it, little significant precipitation falling through the lower layers just ahead of the front, and therefore less moisture available to help jet development.

5. Conclusions

1. Shears below 5000 ft occurred in two main bands: (a) within the boundary layer (below 2000 ft AGL) where values up to 28 kn/1000 ft were recorded (15 March 1988) and (b) close to the low-level jet in the region of 3000 to 4000 ft AGL. Core wind speed maxima in this jet varied quite widely, a peak value of 70 kn was recorded some 30 miles ahead of the front on 15 March 1988.
2. In the zone 4000 to 5000 ft which lies above and beyond the effects of the low-level jet, shears were fewest and most short-lived.

3. The most persistent shear was found in the lowest layers where such shears also occurred most frequently. A secondary frequency peak was evident between 3000 and 4500 ft AGL though here it was generally much shorter at under 2 hours duration.

4. Extreme values of vertical wind shear showed little correlation in time or space with their position relative to the cold fronts, but those lying within 2 hours of the front tended to be a little more persistent than those more distant.

References

Browning, K.A. and Pardoe, C.W., 1973: Structure of low-level jet streams of mid-latitude cold fronts. *QJR Meteorol Soc*, **99**, 619–638.
Crossley, 1962: Extremes of wind shear. *Sci Pap. Meteorol Off*, No. 17. London, HMSO.

551.578.7(495)

A severe hailstorm in northern Greece

S.J. Spanos

Greek Agricultural Insurance Institute, Thessaloniki, Greece

Summary

On 15 June 1988, an unusually severe hail storm occurred over northern Greece. This storm produced hail in excess of 5 cm in diameter, and caused considerable damage to the Halkidiki region of Greece and the See of the Greek Orthodox Church on Mt. Athos. Surface observations and radar data archived by the Greek National Hail Suppression Project show that the storm was strongly tied to terrain influences.

1. Introduction

The Summer of 1988, here defined as the period between 15 April through 30 September, was particularly active over Greece. Hailstorms occurred more frequently, and hail was larger than experienced by the Greek National Hail Suppression Project during previous years (Rudolph *et al.* 1989).

The purpose of this paper is to give a brief study of the activity on 15 June 1988 which produced, what is for Greece, exceptionally large hail. The changes which occurred in the synoptic environment over the preceding days are examined in as much detail as possible and the storm is followed across northern Greece through observations and radar data archived as the storm crossed the region.

There are three areas, referred to as Areas 1, 2, and 3, over which hail suppression operations are carried out over northern and central Greece. Areas 1 and 2, the two northern areas shown in Fig. 1, are supported by operations out of Thessaloniki International Airport. Operations for Area 3 are run from the facilities of the Greek Air Force Base at Larisa. The storm complex examined here tracked south-eastwards between Areas 1 and 2.

The synoptic-scale maps of the *European Meteorological Bulletin* indicate that no frontal systems affected

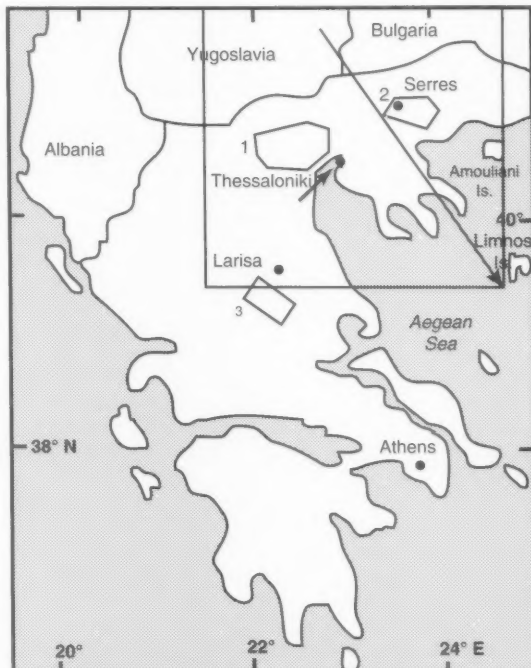


Figure 1. Hail suppression project areas in Greece. The storm track is indicated by an arrow between the project areas.

northern Greece during the period. The surface pressure field was relatively flat with a weak high pressure centre located over the Tyrrhenian Sea (the area between Corsica, Sardinia, Sicily, and Italy). The Cyprus low pressure centre, which forms during the Summer off the south-west coast of Turkey, was just beginning to form.

The mid-troposphere flow, as characterized by the 500 hPa chart, was weak and generally westerly with a broad band of low heights extending from off the west coast of Spain east-north-eastwards to the western part of former Soviet Union. By 0000 UTC on 13 June a jet streak associated with the subtropical jet (STJ) had begun to cross the Mediterranean Sea from Gibraltar to Rome. This jet streak was strengthening in response to ridging over north central Africa. By 0000 UTC on 14 June it extended far enough eastward that north-eastern Greece was located under confluent north-westerly flow. A jet streak in the polar jet stream (PJ) was dropping southwards across central Europe, from Denmark to Austria, and the merger of these two features over the Balkan Peninsula set the stage for strong convection over the region.

At 0000 UTC on the 10th, the STJ was located between the Madeira Islands and Gibraltar. On 11 June it extended from the Canary Islands to south-eastern Spain and by the 13th had advanced to central Italy. By 14 June a well defined STJ existed from the Canaries to central

Italy and then south-eastwards across the Balkan and Asia Minor peninsulas. This orientation placed northern Greece under strong north-westerly flow, and as the PJ streak approached from central Europe and crossed the region on 15 June, Greece was placed under the left rear (entrance) region of the reinforced upper-level jet streak in a zone of upper-level confluence. Given subsequent events, it is safe to assume that this region was conducive to upper-level frontogenesis as is usually the case in such a situation (Holton (1979) p. 239). By 0000 UTC on the 16th, the STJ extended in a well defined band across the Mediterranean. After the 16th, it had drifted far enough south of the project areas that a short-lived lull in convective activity occurred over the next three days as the upper-level flow over Greece took on a more zonal nature. The advance of the jet streaks can be easily followed at the upper (300 hPa) levels as well (Fig. 2).

During the same period, the 850 and 700 hPa charts show the development of ridging in both the height and thermal fields over the Mediterranean. They show that the ridge amplified and drifted eastward from an initial position west of Italy on the 10th to having its axis running along the west coast of the Balkan Peninsula by the 15th (Fig. 3). As the STJ pushed southward on the 16th, the low-level ridge retreated to the west of Italy.

At the surface, on the synoptic scale, a weak high pressure system (1015 hPa) dominated the region over the entire period. This system was centred near Italy with

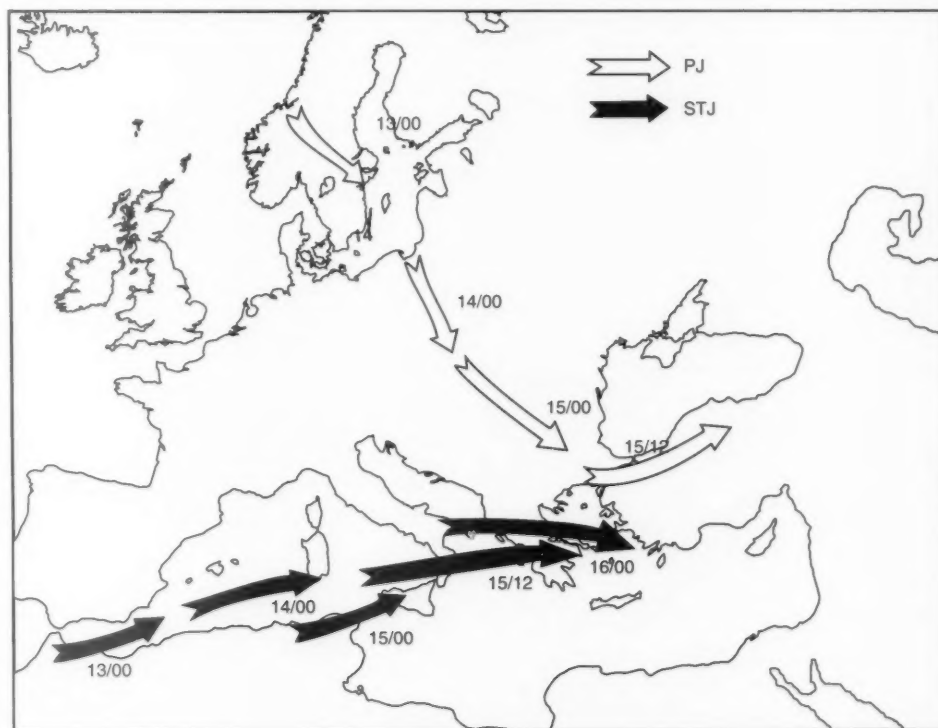


Figure 2. The evolution of the jet streaks between 13 and 16 June 0000 UTC from 300 hPa maximum wind analysis. STJ and PJ indicate the subtropical and polar jets. The numbers related to the arrows are date/time.

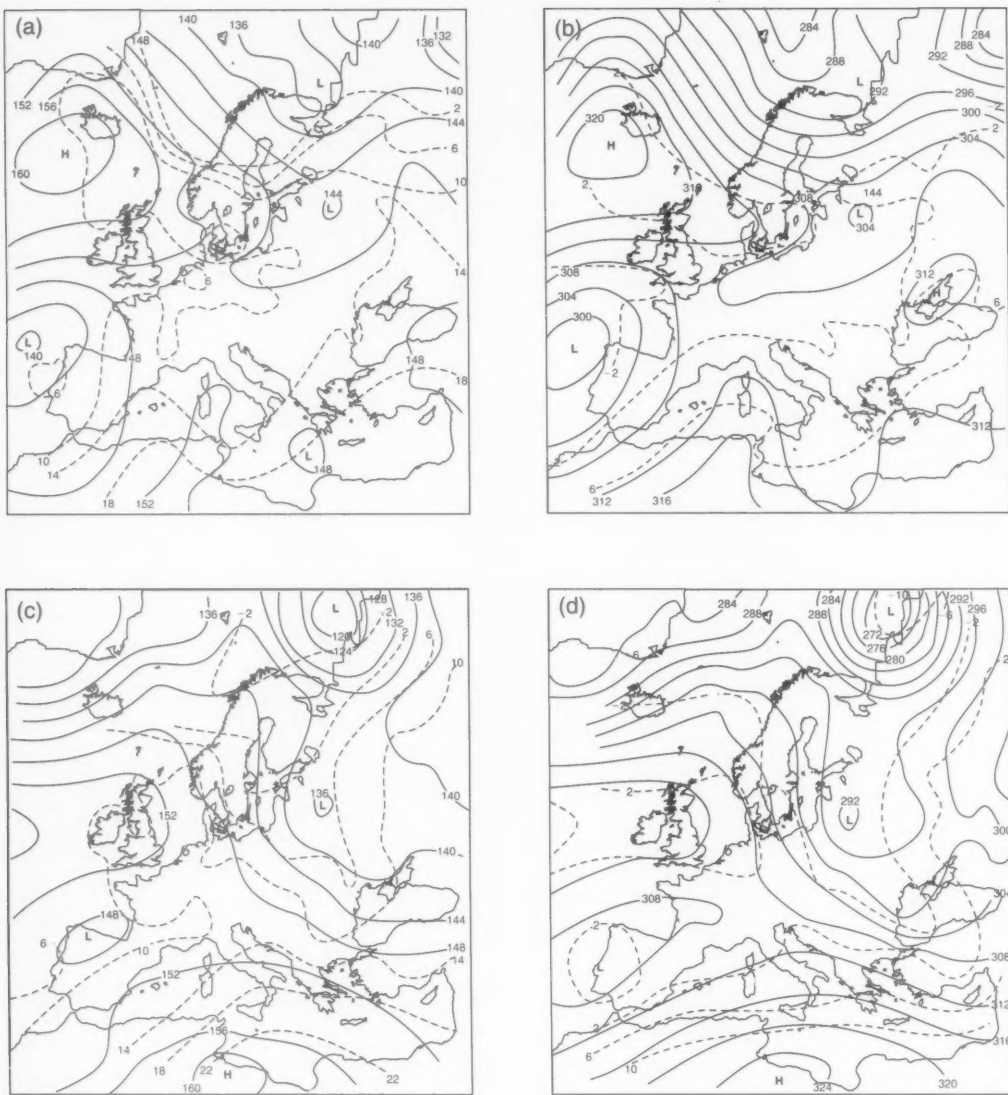


Figure 3. Synoptic analyses adapted from *Meteorological Bulletin* at 0000 UTC, (a) 10 June at 850 hPa, (b) 10 June at 700 hPa, (c) 15 June at 850 hPa, and (d) 15 June at 700 hPa.

the highest pressures usually between the Tyrrhenian Sea and the Gulf of Sidra. As mentioned, the maps of the *European Meteorological Bulletin* show no significant frontal activity over the Mediterranean during the period. This picture changes, however, as one focuses on the sub-synoptic scale.

3. Sub-synoptic-scale analysis

3.1 Surface analysis

At 0000 UTC on the 13th a detailed (2 hPa interval) analysis of the surface chart (not shown) revealed the development of an inverted trough over the Adriatic Sea. This trough was probably a hydrostatic response to the advance of the 850 and 700 hPa thermal ridges

mentioned earlier. By 0000 UTC on the 14th, in response to the surface pressure falls, the advance of the low- and mid-level thermal ridges, and the development of confluent, frontogenetic flow aloft, a boundary was beginning to form along a line between Rome and Athens. Closed low-pressure centres were found near both of these locations.

At 0000 UTC on the 15th (Fig. 4) this distinctly warm-frontal boundary was found along the east coast of the Adriatic. The low near Athens had weakened and drifted northward to near Larisa. At the same time, a second region of frontogenesis had developed north and west of the Black Sea as a weak polar front advanced south-eastward ahead of the polar jet streak (Fig. 5).

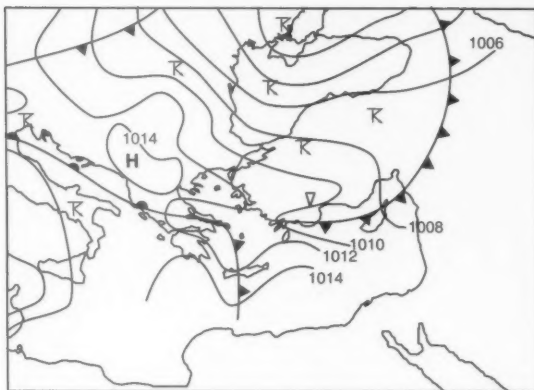


Figure 4. Subjective 2 hPa surface analysis at 0000 UTC on 15 June.

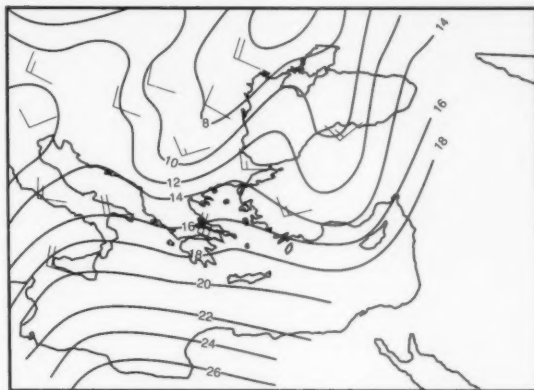


Figure 5. Subjective 2-degree 850 hPa analysis of thermal field at 0000 UTC on 15 June.

The evolution in space and time of the two systems can be better followed in a series of 1 hPa surface analyses every three hours (Fig. 6). The analyses showed a number of sub-synoptic features (squall lines and bubble highs) which affected the northern Balkans. The stationary front over western Greece at 1200 and 1500 UTC retreated as the cold front advanced from the north. By 1800 UTC the two fronts had merged over Greece and the low over Larisa had drifted southwards to be over the Aegean Sea.

Between 0900 and 1200 UTC the pressure at Thessaloniki dropped 2.1 hPa as the cold front approached from the north. Both pressure traces for Thessaloniki and Serres indicate the front passed near 1500 UTC (Fig. 7).

3.2 Thermodynamic aspects

The 0600 UTC Thessaloniki sounding indicated instability with a subsidence inversion at 550 hPa and a weak frontal inversion at 850 hPa. Strong winds were observed aloft. With the advance of the short wave from north-west, the temperatures dropped in the layer between 550 and 300 hPa. An increase in temperature due to differential advection was observed in the layer between 850 and 700 hPa and the levels below 850 hPa were approximately dry adiabatic. The effect of these temperature changes in the 1200 UTC sounding, in combination with an increase in moisture below 700 hPa, enhanced the pre-existing instability (Fig. 8). A slight backing of the winds between 700 hPa (300/41) and 600 hPa (290/52) was enough to cool the layer at an intense rate of $0.7^{\circ}\text{C h}^{-1}$, smoothing the inversion observed in the 1200 UTC sounding. After approximately five hours a 3.5°C drop in the mean layer temperature was confirmed by the patrolling aircraft (Fig. 8). The high levels of instability and wind shear were strong indications of severe weather.

3.3 Radar history and storm-related events

At 0300 UTC on 15 June 1989, stratiform clouds were widespread over northern Greece. Radar indicated the tops of these clouds to be generally 2 km or less. By 1000 UTC convection had begun to be detected over Bulgaria with reflectivities reaching 40 dbz and tops extending to near 8 km. At 1430 UTC cells were detected over Yugoslavia at a range of 110 km from Thessaloniki. These cells were moving very rapidly toward the south-east, reflecting the strong north-west flow over the region associated with the PJ. Speeds reached 30 kn as the storms moved south-eastwards. While predominant cell motion followed the 700 hPa wind direction, the storm motion deviated 20° to the right of the mean tropospheric wind. At the same time reflectivities between 35 and 40 dbz were measured at altitudes between 4 and 4.5 km and tops reached 9 km. Convection then began to develop rapidly and by 1512 UTC a cluster of cells extended from Lake Doirani to Lake Kerkini (Fig. 9). Two 48 dbz reflectivity maxima were present by this time and tops had climbed to 10 km. Two villages between these lakes reported hail damage to crops the next day.

As these cells moved between Project Areas 1 and 2, they continued to intensify. Fig. 13 is a photograph taken from Thessaloniki International Airport showing the appearance of the storm at 1647 UTC. Fig. 10 gives some indication of the appearance of the storms on radar at this time. The storm in Fig. 13 is seen as the 60 dbz maximum in the south-eastern quadrant of Fig. 10. The same figure shows a second cluster of cells located north-north-west through north of the radar site. This activity moved along nearly the same track as the first cells. The weak returns south-west to north-west and south-east of the radar are ground clutter, the 38 dbz core in the south-west quadrant is Mt. Olympus. Fig. 9 is a time-position plot of the activity as it crossed north-eastern Greece.

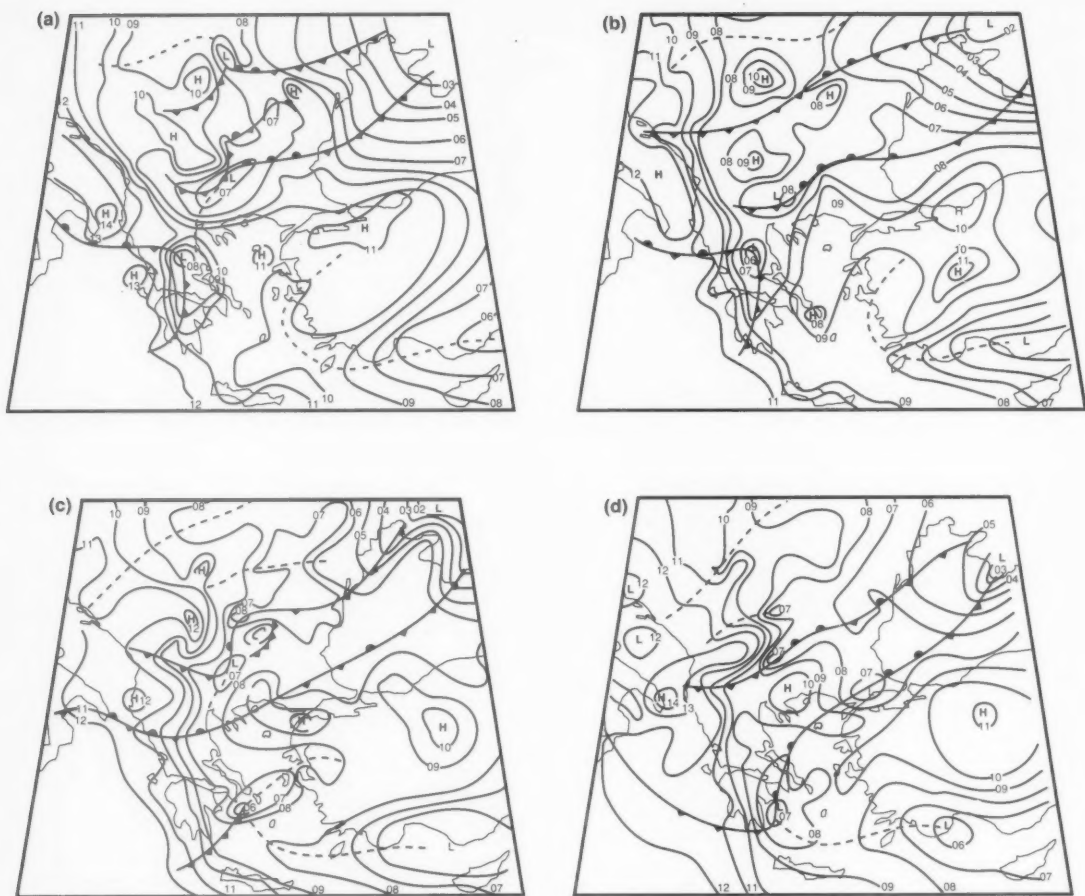


Figure 6. Subjective 1 hPa surface analyses for (a) 1200, (b) 1500, (c) 1800, and (d) 2100 UTC on 15 June. Dashed lines represent pressure troughs.

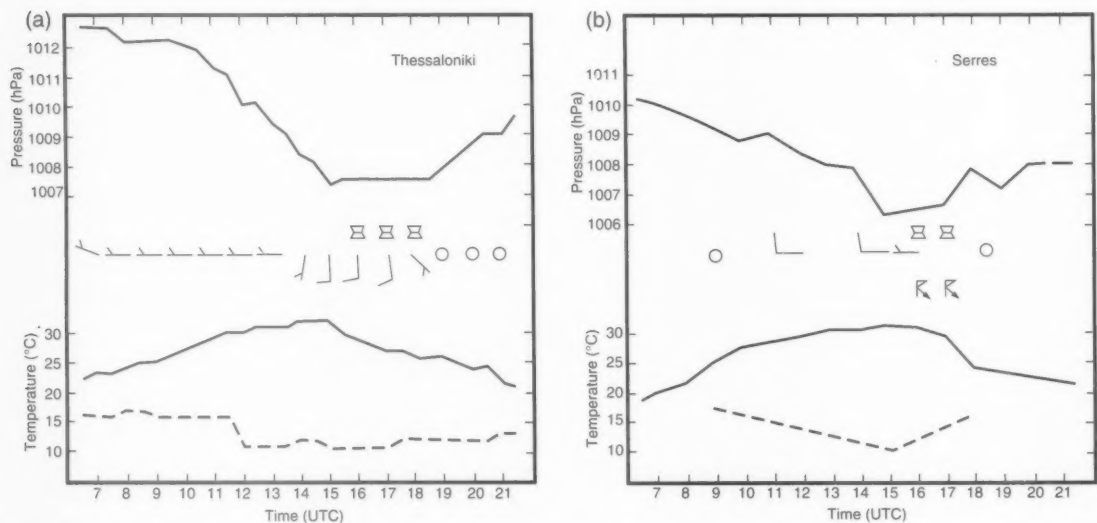


Figure 7. Time section based on surface observation of pressure, temperature, dew-point, wind, and weather for (a) Thessaloniki and (b) Serres stations.

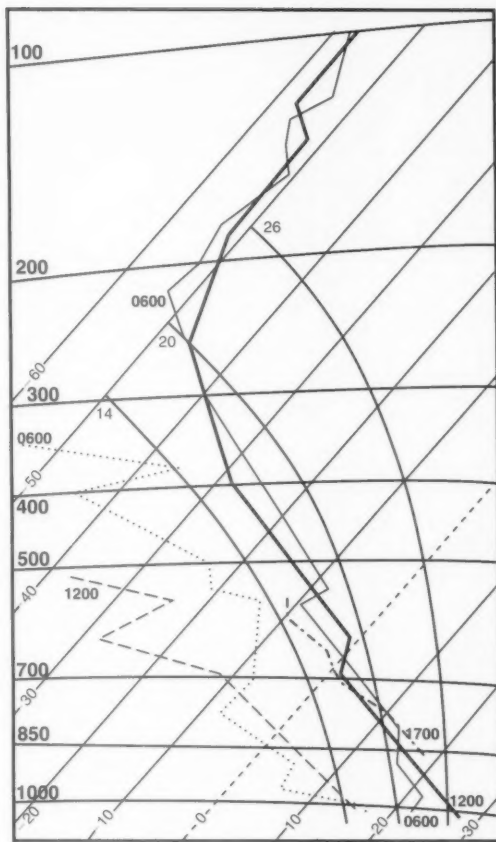


Figure 8. Thessaloniki soundings on 15 June for 0600 and 1200 UTC and the aircraft temperature measurements at 1700 UTC (dashed-dot line). The dotted and the dashed lines are dew-point traces at 0600 and 1200 UTC, respectively.

Close study of the archived data shows that the cells generally intensified when in the immediate vicinity of mountains, especially if they tracked along a south-facing slope. Further, the cells weakened noticeably when they passed over the Gulf of Ierissos. While this is only one case documented and examined in this detail, it is strong support for coupling convective activity and topography over the region.

The surface divergence field shown in Fig. 12 for 1500 UTC reflects some of these terrain influences. The two convergence maxima (negative centres), related to the approach of the cold front (Fig. 6(b)), are separated by a divergence area over the Gulf of Thessaloniki. This is to be expected and is due to the sea breeze effect, which is strongest by this time. A diffluent zone is usually developed as the breeze winds blow approximately normal to the coast. The extension of the convergence maximum, east of Thessaloniki over Halkidiki peninsula, can be attributed in a similar way to the sea breeze effect. At 1800 UTC the weak divergence centre over the same region is probably related to the low-level storm outflow. This is one reason for the more westerly path of the

second storm. Another reason for the difference in paths may be that west-facing mountain slopes at that time were a more favourable place for storm formation.

After crossing the Gulf of Ierissos, the cells reintensified with the largest hail of the day being reported from Amouliani Island at approximately 1800 UTC (Fig. 14). Fig. 11 is a radar image of the storm at the time maximum hailstones was reported. Echo appearance is similar to that called 'fingers' and is considered to be reflections from the hail shafts (Grebe (1982) p. 55). The reflectivity core continued to move south-eastward along the Mt. Athos peninsula where considerable damage occurred. By 1900 UTC, the cells were 120 km south-east of Thessaloniki, approaching Limnos Island, which reported a thunderstorm with winds gusting to 40 kn at 2000 UTC with 32 mm of rain between 1925 and 2010 UTC.

A total of 22 villages along the 150 km path of the storm reported hail damage. On Amouliani Island alone, over 500 houses and 200 cars were badly damaged by hailstones in excess of 5 cm in diameter. While such levels of damage are not unknown in Greece, the size of the hail and the extent of the damage produced by the storm were exceptional by local standards.

4. Conclusion

A number of synoptic and local factors were responsible for the severity and extent of hail which occurred on the evening of 15 June 1988. The meteorological features can be summarized as follows:

- The convergence of subtropical and polar jet streaks over the Balkans established the conditions favourable for the enhancement of convection.
- The peak of activity which occurred at 1800 UTC was related to the strong cold advection in the mid-levels which continuously acted as a destabilization mechanism for more than five hours. The trigger was provided by the advance of the cold front.
- The storm of 15 June 1988 was a multi-cellular storm with right deviation of the storm motion vector relative to the mean tropospheric wind.
- Radar PPIs recorded during the hail fall support the relationship between 'fingers' and ground observation of hail.
- Specific characteristics of storm evolution can be explained by topographic influences on storm propagation and intensity. The storm complex slowed when it reached the coast, especially the diffluent zone produced by the sea breeze around a bay. The activity peaks over the south-facing mountain slopes can also be attributed to the warmer air over the inclined ground.
- A surface analysis at 2 hPa and an analysis of the 850 hPa thermal field at 2 °C resolution is necessary to reveal significant features of the summer weather on a continental scale. A surface analysis at 1 hPa is necessary to relate mesoscale and radar features.

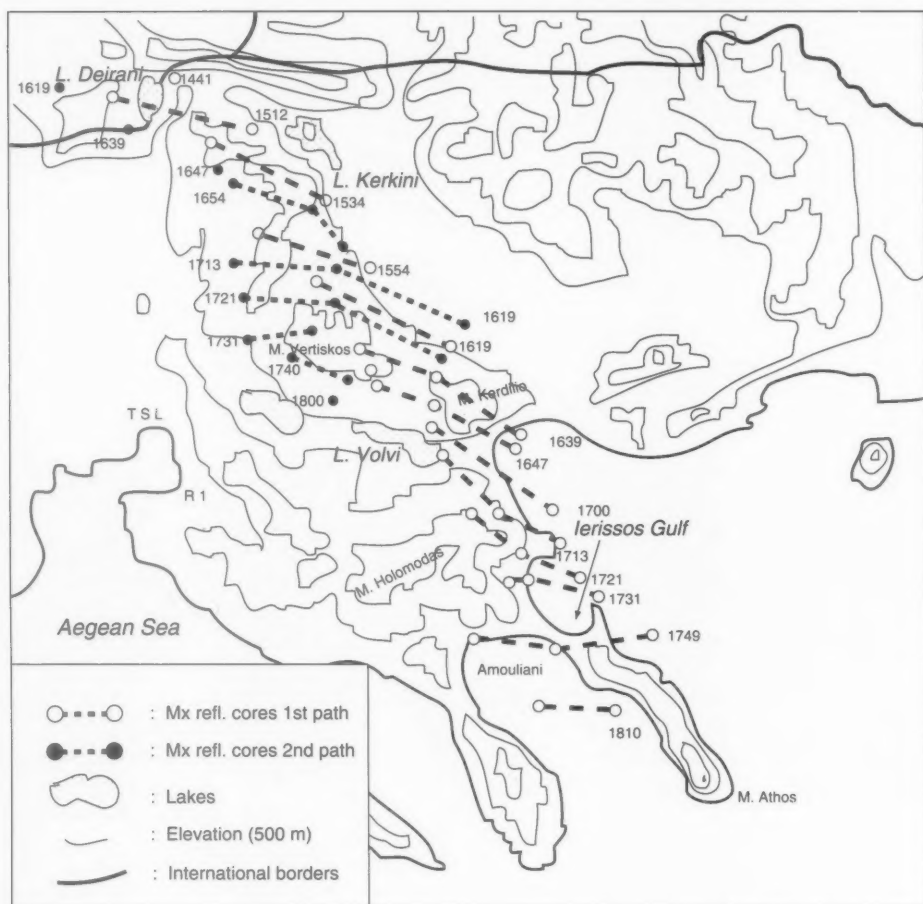


Figure 9. Time-position plot of the maximum reflectivity cores for the two storm complexes. The cores are connected with dashed lines for the first path and dotted lines for the second.

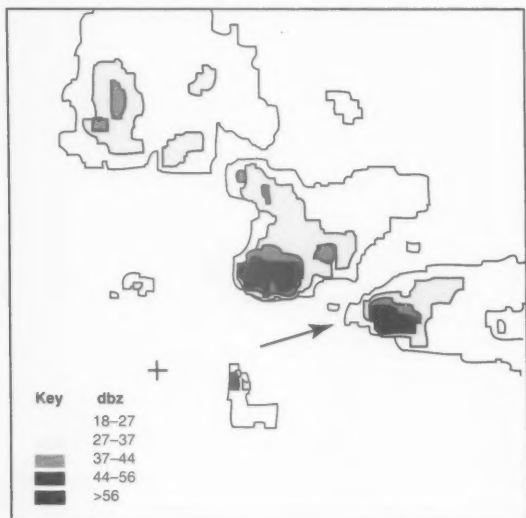


Figure 10. Radar image at 1647 UTC showing the two storm complexes. Arrow indicates storm in Fig. 10.

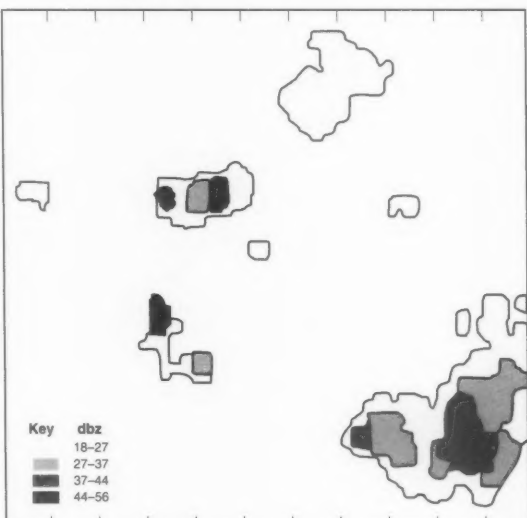


Figure 11. Radar image at 1758 UTC showing the appearance of the echo at the time of maximum recorded hail fall.

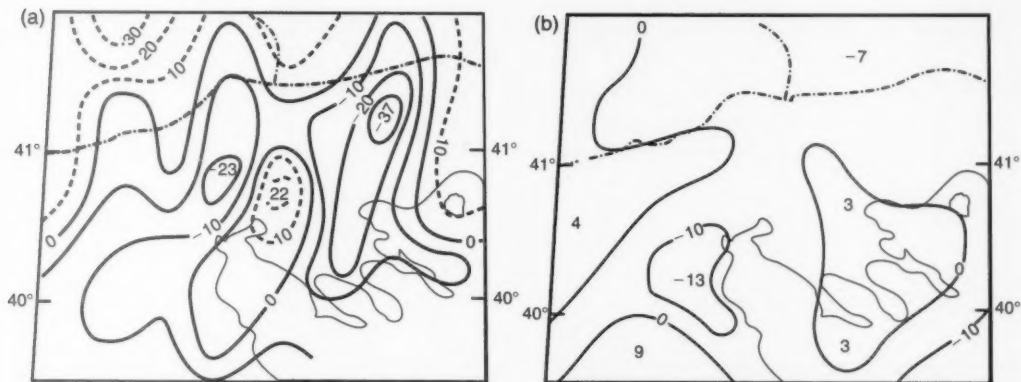


Figure 12. Surface divergence fields calculated from surface wind data at (a) 1500 and (b) 1800 UTC ($s^{-1} 10^{-5}$).



Figure 13. Photograph taken from Thessaloniki at 1645 UTC showing the first storm complex.



Figure 14. Photograph (taken on the morning of 16 June) of a refrigerated hailstone.

References

Grebe, R., 1982: An outline of severe local storms with the morphology of associated radar echoes. NOAA Technical Memorandum NWS TC 1, US Department of Commerce, Rockville.

Henderson, T.J., 1986: The hail suppression program in Greece, 10th Conference on Weather Mod., American Meteorological Society, Arlington, 342-347.

Holton, J.R., 1979: An Introduction to dynamic meteorology, second edition. International Geophysics Series, Vol. 23, Academic Press, NY.

Rudolph, R.C., Krauss, T.W., Sackiw, C.M. and Davis, A.G., 1989: Greek National Hail Suppression Program 1988 Annual Report. Prepared by INTERA Technologies, Ltd. for National Agricultural Insurance Institute (ELGA). Available from ELGA Patisio 30 Athens 10170.

European Meteorological Bulletin 1988: Vol. 13, Numbers 162-168. Offenbach, Germany, Deutscher Wetterdienst.

Polar lows over the North Atlantic

G.C. Craig

Joint Centre for Mesoscale Meteorology, University of Reading

A prolonged cold air outbreak over the North Atlantic on 6–11 January 1991 provided examples of many different types of polar lows. The different structures and locations within the air mass of these systems reflect the different physical processes that are believed to be responsible for their genesis and intensification. At least three distinct types of polar low (labelled A, B, and C) are visible on the single infrared image in Fig. 1. Fig. 2 shows 900 hPa absolute vorticity (colour) and wet-bulb potential temperature (contours) taken from an operational analysis of the UK Met. Office fine-mesh model, at a time three hours before the satellite image.

System A is a comma-shaped cloud pattern, whose formation was initiated by a large amplitude, upper-level short wave. The life cycle of such systems is similar to

that of many large-scale baroclinic cyclones, despite the weakness of the low-level thermal gradients in the cold air mass. The small amplitude of the 900 hPa perturbation associated with this system is apparent in Fig. 2, especially when contrasted with the frontal cyclone (labelled AA), located just to the east. Release of latent heat can substitute for low-level thermal advection, producing a development that closely resembles the usual baroclinic pattern (Craig and Cho 1992). The two vortices labelled B in Fig. 1 formed along a shallow shear zone, or 'arctic front'. This is visible as a region of high vorticity and warm θ_w in Fig. 2, which indicate the presence of high moist potential vorticity. Such strips are barotropically unstable and can rapidly roll up into a train of small cyclones (Joly and Thorp 1990).

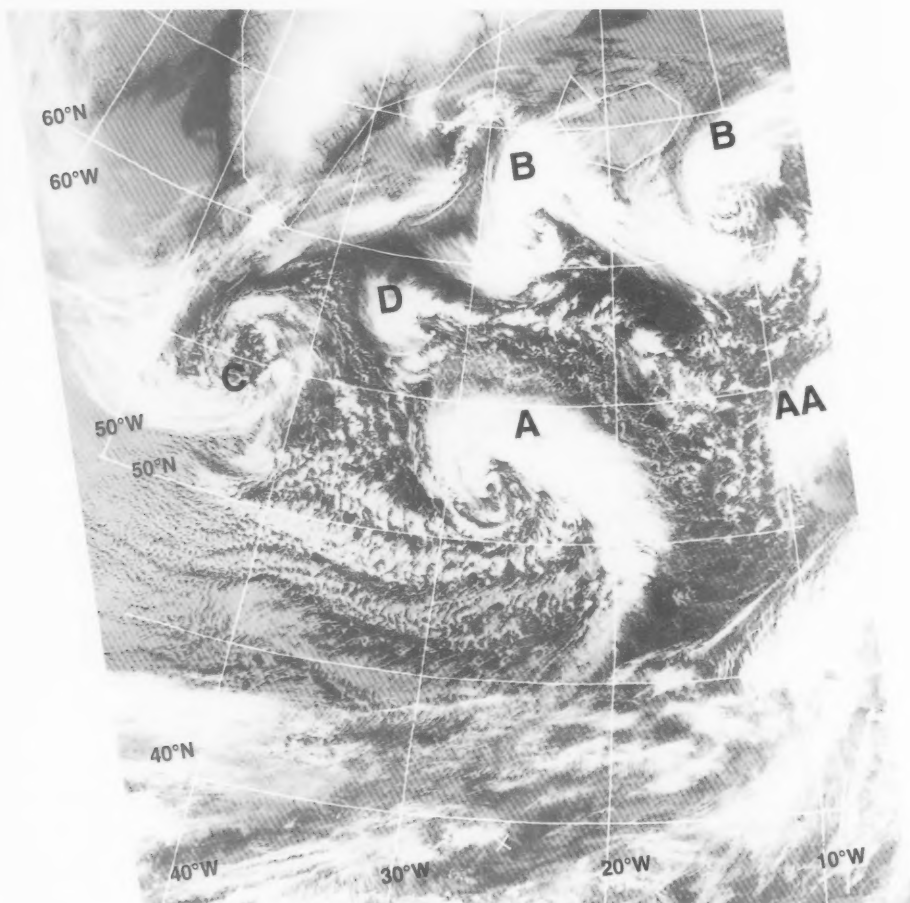


Figure 1. NOAA 11 infrared satellite image for 1526 UTC on 8 January 1991. Letters identify cloud systems referred to in the text.

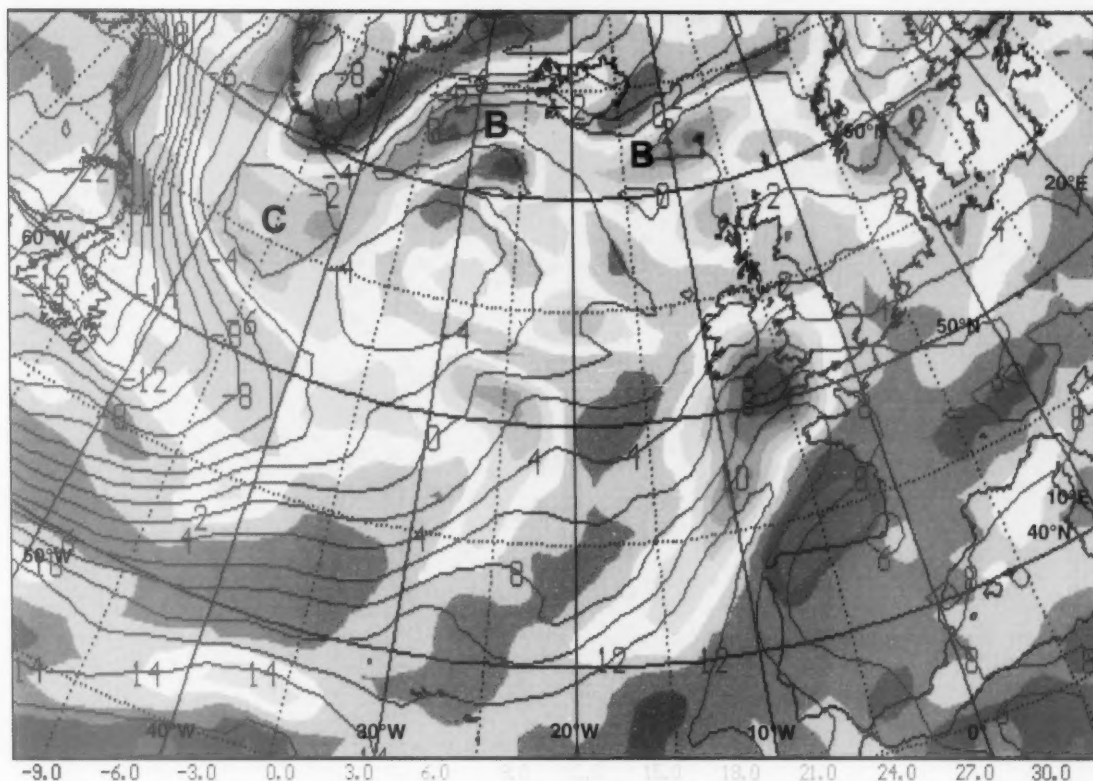


Figure 2. Absolute vorticity and wet-bulb potential temperature θ_w at 900 hPa for 1200 UTC 8 January 1991. Absolute vorticity is shown by colour shading, with the scale at the bottom of the figure; for example, yellow shading indicates vorticity in the range $12-15 \times 10^{-5} \text{ s}^{-1}$. Contours show θ_w (interval 2 K).

The genesis of vortex C appears to be intimately associated with orographic effects. Two patches of high vorticity formed to the east and west of Greenland, then merged at the tip and were shed off into the Atlantic. The two maxima are still visible at the time of Fig. 2. For a period of about twelve hours, the vorticity decayed as the vortex moved southwards, but then reintensified, apparently due to enhanced convection as the system passed over warmer water. The vortex persisted as it moved south and then eastwards, arriving three days later over the United Kingdom. The structure at this later time was discussed by Grant (1991). At no point in its development did the system appear to be associated with any upper-level forcing, and except at the genesis stage near Greenland there was no significant baroclinicity.

As discrepancies between the satellite image and vorticity analysis suggest, a major difficulty in studying and forecasting polar lows is the lack of high-resolution data. In the case of small vortices such as the one labelled D in Fig. 1, very little is known at all.

References

Craig, G.C. and Cho, H.-R., 1992: A study of two cases of comma cloud cyclogenesis using a semigeostrophic model. *Mon Weather Rev.* **120**, 2943-2961.
 Joly, A. and Thorpe, A.J., 1990: Frontal instability generated by tropospheric potential vorticity anomalies. *QJR Meteorol Soc.* **116**, 525-560.
 Grant, J.R., 1991: Satellite and radar photographs — 11 January 1991 at 0300 and 0316 UTC. *Meteorol Mag.* **120**, 58-60.

World weather news — July 1993 — apology

A gremlin caused the deletion of tropical storm No. 6; please insert

6

Nathan

NWP

19 Jul

25 Jul

70.

Regrettably there is no room for World weather news in this or the December issue.

Infrared imagery showing upper-level waves —

3 May 1993

T.D. Hewson

Joint Centre for Mesoscale Meteorology, University of Reading

Figs 1 and 2 show the circulation and frontal systems associated with a large North Atlantic depression. The cold front is particularly marked, extending over at least 3500 km, from about 25° N, 50° W to about 65° N, 25° W. Data from the UK Met. Office limited area model (LAM) in Fig. 2 indicates that at low levels along the length of this front there are both strong thermal gradients (changes in 900 hPa wet-bulb potential temperature of up to 18 °C in 500 km), and a 'classical' deformation pattern (as shown by the splaying out of isobars in the cold air, when looking in a south-easterly direction). Theoretical work (e.g. Schar and Davies (1990)) suggests such features are conducive to the initiation of surface frontal waves (although continued development requires the relaxation of the deformation pattern). The LAM data does in fact hint at two surface

waves, near 48° N, 37° W and 61° N, 26° W. Whilst high-resolution models regularly generate frontal waves in circumstances such as this, the sparsity of surface observations over oceans often makes their existence difficult to verify. In such instances forecasters commonly use satellite imagery to aid the surface analysis. The imagery in Fig. 1 is broadly consistent with the position of the LAM waves, showing colder cloud-tops just south-west of Iceland, and a prominent bump in the cloud mass centred around 49° N, 40° W.

Closer inspection of Fig. 1 shows there are in fact two bulges in the cloud mass near 49° N, 40° W (marked by black dots). In a 21-hour animation of hourly Meteosat images (centred around the time of Fig. 1) it was possible to identify five discrete bulges such as these; all of which developed between 45° N and 50° N, translated rapidly

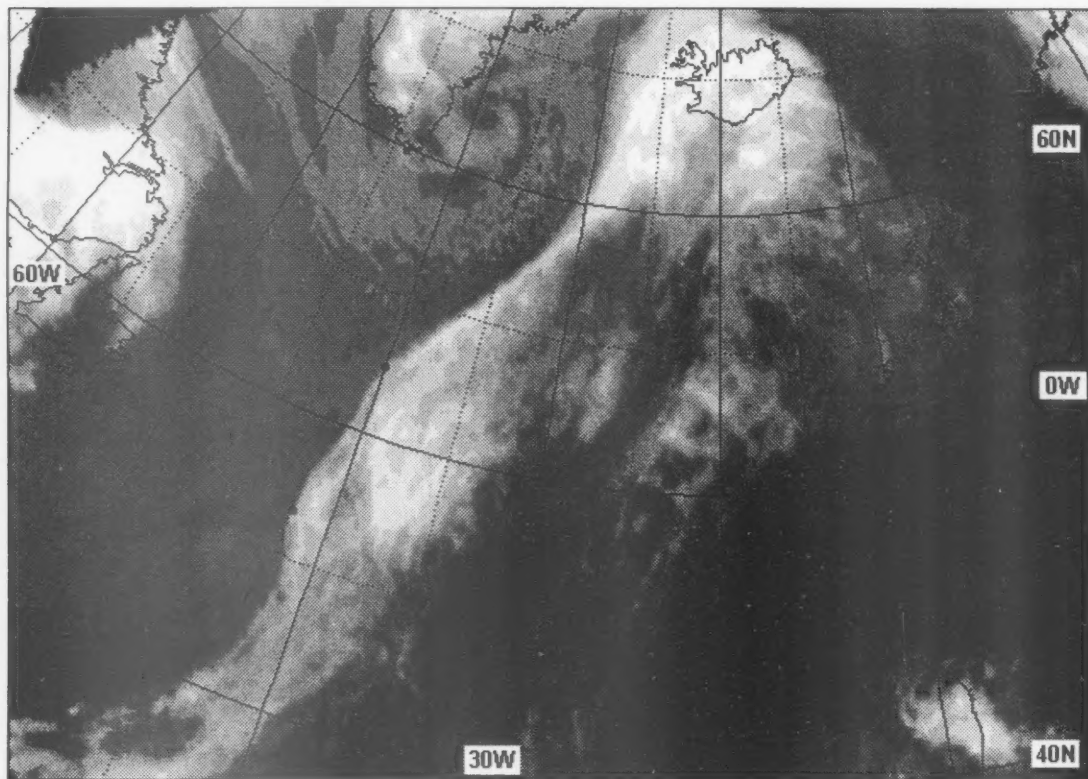


Figure 1. Meteosat infrared image for 2100 UTC on 3 May 1993. Black dots near 50° N, 40° W indicate the tips of two bulges in the cold front cloud band. These appear to be upper-level waves (see text).

The Meteorological Magazine November 1993

ISBN 0 11 729348 2

CORRECTIONS

Page 281, Figure 2

see replacement below (original version too indistinct)

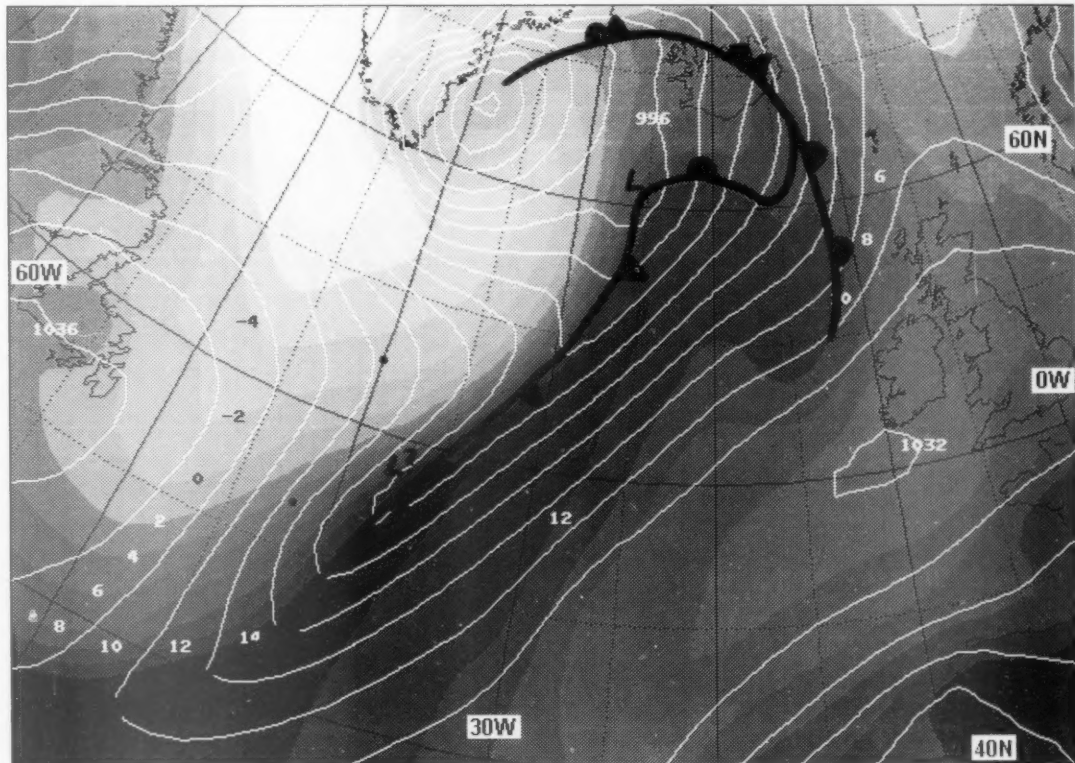
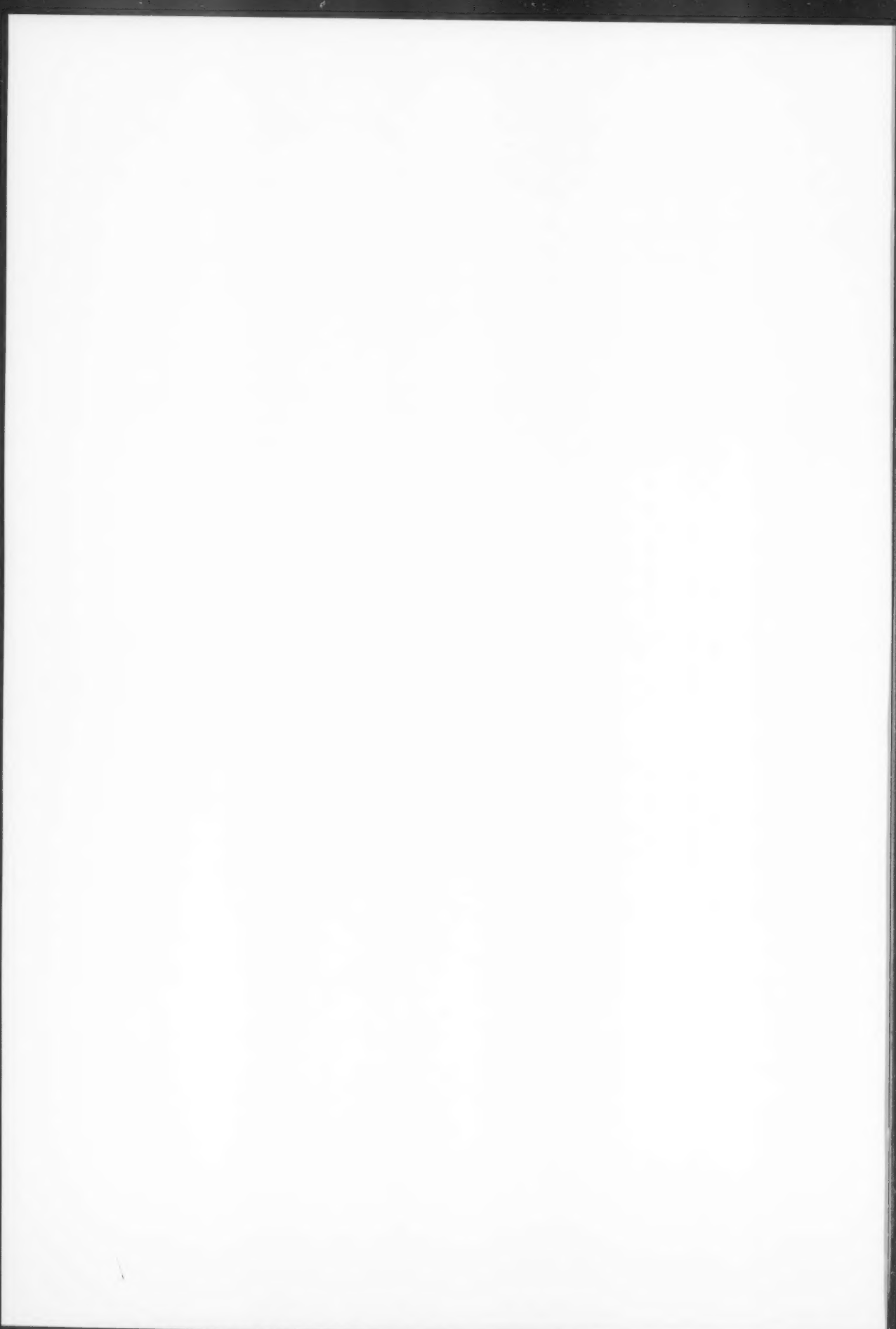


Figure 2.

*Meteorological Office
December 1994*



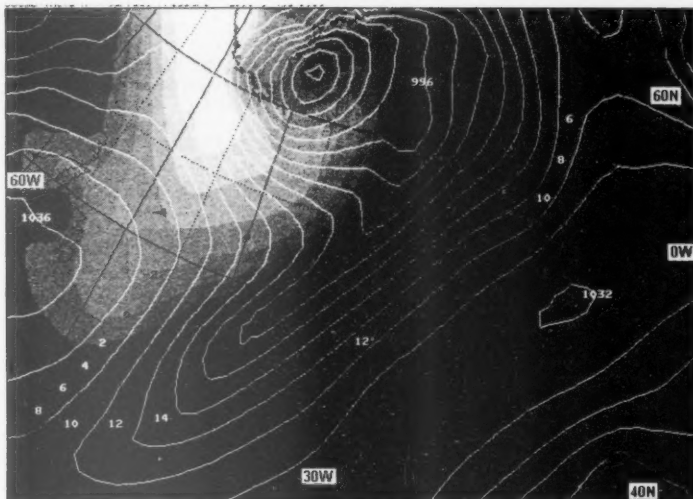


Figure 2. LAM data for 2100 UTC on 3 May 1993 (a 3-hour forecast based on the 1800 UTC analysis). Shading indicates wet-bulb potential temperature at 900 hPa. Each shade covers a 2°C range, using darker shades for higher values. White contours show surface pressure at intervals of 4 hPa. Black dots are as in Fig. 1.

north-north-east, and then disappeared between 50° N and 55° N. Fig. 3 shows the tracks of the tips of each of these*.

In chapter 4 of *Images in Weather Forecasting* (Bader *et al* 1994) it is suggested that satellite image sequences can help in distinguishing between frontal waves extending throughout the troposphere and those confined to upper levels. Whilst convex bulges in the cloud mass of a frontal zone are characteristic of both, what differentiates an upper-level wave is that these bulges (i) move rapidly along the upper flow, and (ii) have a relatively short life-time.

The tracks in Fig. 3 satisfy both these criteria. Mean tip speeds range from 60 to 120 knots, whilst life-times range from 2 to 10 hours. Additional LAM data for 2100 UTC (not shown) for the upper troposphere (at 300 and 500 hPa) indicates winds whose direction and speed are very similar to those of the tracks in Fig. 3. This too suggests the waves are upper-level waves.

*As no satellite data were available between 0900 and 1130 UTC on the 4th the progression after 0900 UTC of the fifth track is not known.

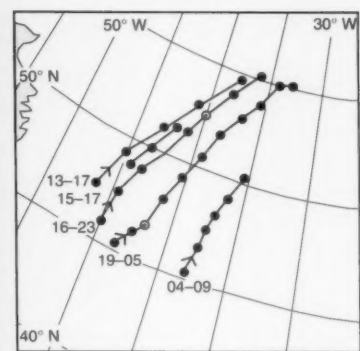


Figure 3. Tracks of upper-level waves between 1200 UTC on 3 May 1993 and 0900 UTC on the 4th. Dots show positions, at hourly intervals, of the tips of bulges in the cold front cloud band. These were tracked using animated Meteosat infrared imagery. Text indicates the time span (UTC) covered by each track. The two ringed dots are those depicted in Figs 1 and 2.

The surface wave at 48° N, 37° W hinted at in Fig. 2 was monitored using further LAM data, at 3-hour intervals for 0000 through to 1200 on the 4th. It appeared to move south-south-east, developing into a cut-off low around 42° N, 35° W, whilst the existence and history of this wave cannot be verified using surface observations, it is nevertheless clear that the motion portrayed within the model is very different to that of the cloud bulges shown in Fig. 3.

Thus whilst the image in Fig. 1 seemed to indicate the presence of surface frontal wave(s) in mid-Atlantic (around 49° N, 40° W), further investigation using animated hourly images has shown that this impression is probably incorrect. The cloud bulges are more likely to be symptomatic of only upper-level waves.

References

Bader, M.J., Forbes, G.S., Grant, J.R., Lilley, R.B.E. and Waters, A.J. (1994): *Images in Weather Forecasting — a practical guide for interpreting satellite and radar imagery*. Cambridge University Press. To be published late 1994.
 Schar, C. and Davies, H.C., 1990: An instability of mature cold fronts. *J Atmos Sci.* **47**, 929–950.

Use of Willmott's index of agreement to the validation of meteorological models

V. Badescu

Mecanica, Termotehnica, Polytechnic Institute of Bucarest, Bucarest 79590, Romania

Summary

An important aspect of the meteorological model development process is the evaluation of model performance. In this paper we made a discussion about the estimations provided by the Willmott's index of agreement d_2 as compared to those predicted by other more usual statistical indicators. The results we present were obtained during the validation of a simple empirical relationship between cloud shade (CS) and point cloudiness (PC). 1740 pairs of monthly average values (CS, PC) from 29 weather stations in Romania were used. Generally, the index of agreement was found out to be in good concordance with the other indicators. However, some non-concordances were observed when a finer analysis was considered.

1. Introduction

The evaluation of model performance is an important aspect of the model development process. For this reason, the evaluation of methods that may be used to determine and compare the accuracy of models is of primary concern. In the field of meteorology sound work on this subject was performed by Willmott and co-workers (Willmott 1981, 1982, 1984, Willmott *et al.* 1985) and by other authors (e.g. Fox (1981, 1984), Preisendorfer and Barnett 1983, Won 1984, Zwiers and Thiebaut 1987, Hanna 1989, Lorimer 1989, Ross and Fox 1991).

There is a general point about the use of verification that is important to recognise. Because there are different meteorological communities (e.g. modellers, forecasters, customers) interested in the results, there is a genuine need for different sorts of statistics to be used to present verification results. Of course, these different statistics represent different ways of packaging the same information from the variables involved in verification. However, each packaging now in use has some worthwhile advantage which persuaded a certain community of users to adopt it. As we know, the correlation- and skill-based indices are now in widespread use. In the latter, time difference or error measures were strongly recommended to be used during the valuation of models (Willmott 1985). Sometimes non-dimensional indices are required. In order to avoid some difficulties raised by the existing adimensionalization procedures, Willmott (1984) proposed two new non-dimensional statistical indicators, d_1 and d_2 , named 'indices of agreement'.

In this paper we intend to make a brief comparison between the estimations provided by some usual difference measures, on one hand, and the index of agreement d_2 . The results we present here were obtained during the validation of an empirical relationship between cloud shade and point cloudiness.

2. Empirical relationship of cloud shade to point cloudiness

Many authors reported on the empirical relationship between cloud cover and bright sunshine (Reddy 1974, Rangarajan *et al.* 1984, Harrison and Coombes 1986). Their studies are of a special interest for the solar radiation computing methods developed on the basis of long-term averages of bright sunshine (e.g. the International Energy Agency (IEA 1984)) because sunshine records are not always kept at weather stations, but long-term records of observed total cloud cover are available for most observing stations of the world. Recently, we reported on the empirical relationships between cloud cover and bright sunshine for the Romania climate and latitudes (Badescu 1990). For a given period of time (say a month) we denote by S and PC (point cloudiness) the ratio between the actual and the maximum possible number of hours of bright sunshine and the average total cloud amount (in tenths) observed by eye, respectively. The complement of S is often called cloud shade $CS=1-S$. The three simple relationships we previously analysed have the following forms:

$$CS = a_1 + b_1 PC \quad (1)$$

$$CS = a_2 PC + b_2 PC^2 \quad (2)$$

$$CS = a_3 PC + b_3 PC^2 + C_3 PC^3 \quad (3)$$

where a_i , b_i ($i=1, 2, 3$) are regression coefficients whose values were determined by a least squares fit of the Equations (1-3) to the observed values of cloud shade (CS_{obs}). Once a_i , b_i were obtained, the three equations were used to compute new values of cloud shade (CS_{comp}).

In this paper we refer exclusively to the simple relationship given by Equation (2). Note that this non-

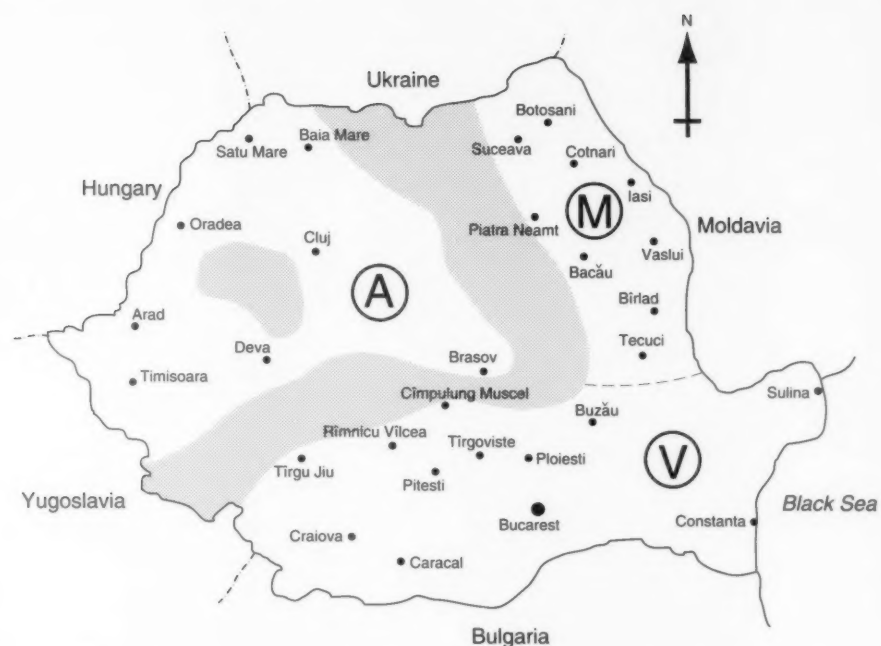


Figure 1. Locations of the 29 Romanian weather stations where the relationship of cloud shade to point cloudiness (Equation (2)) was verified. The dashed area shows the Carpathian Mountains. The three historical Romanian provinces are: A — Ardeal, M — Moldavia, V — Valahia.

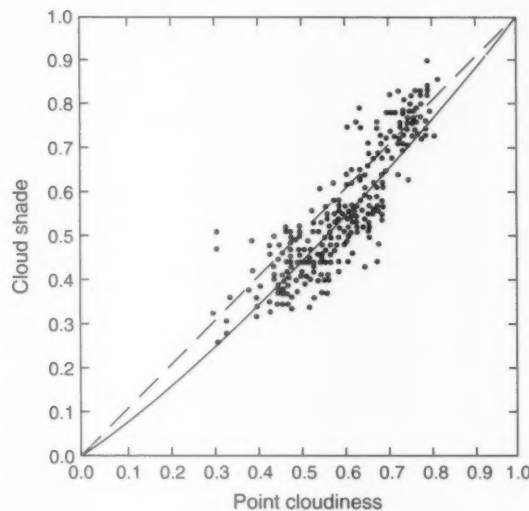


Figure 2. Cloud shade (CS) versus point cloudiness (PC) for 29 Romanian weather stations (5-year monthly average values).

linear formula was also preferred by Rangarajan *et al.* (1984) and Harrison and Coombes (1986).

3. Data basis and statistical indicators of accuracy

Meteorological data were collected from 29 Romanian weather stations selected to give a broad coverage of the

country in both latitude and longitude (Fig. 1). In computations we used 1740 pairs of PC/CS monthly average values from a five-year interval. The 348 multi-year monthly average values are shown in Fig. 2. Note that some of these values are superposed.

First, the accuracy by which the Equation (2) evaluates the monthly average values of CS was verified by using three usual statistical indicators of accuracy, namely the mean bias error (MBE), the second centred moment of the error distribution (S_D) and the mean absolute error (MAE) given by:

$$MBE = (1/N) \sum_{i=1}^N (CS_{\text{comp},i} - CS_{\text{obs},i}) \quad (4)$$

$$S_D = (N-1)^{-1} \sum_{i=1}^N (CS_{\text{comp},i} - CS_{\text{obs},i} - MBE)^2 \quad (5)$$

$$MAE = (1/N) \sum_{i=1}^N |CS_{\text{comp},i} - CS_{\text{obs},i}| \quad (6)$$

where N is the number of monthly average values. Second, we computed the index of agreement d_2 , defined by Willmott *et al.* (1985) as:

$$d_2 = 1 - \frac{\sum_{i=1}^N (CS_{\text{comp},i} - CS_{\text{obs},i})^2}{\sum_{i=1}^N (|CS_{\text{comp},i} - m_{CS_{\text{obs}}}| + |CS_{\text{obs},i} - m_{CS_{\text{obs}}}|)^2} \quad (7)$$

where $m_{CS_{\text{obs}}}$ is the mean of the observed values of CS . The index of agreement varies between 0.0 and 1.0 where a value of 1.0 expresses perfect agreement between CS_{comp} and CS_{obs} and 0.0 describes complete disagreement.

4. Results and discussions

We applied Equation (2) to compute cloud shade by using only meteorological data from each of the three historical provinces of Romania. Table I shows the results. The empirical relationship we tested has close enough performance on the whole of Romania. This can be verified by means of any of the four indicators we used. Note that all three 'classical' indicators (MBE , S_D and MAE) agree with the fact that the simple relationship we tested has the worst performance in Valahia. However, the index of agreement d_2 does not recognize this fact.

Next, we tested the four statistical indicators to study the accuracy of the Equation (2) when applied in areas other than the one where the regression coefficients were determined. First, we analysed the accuracy of the regression formula that we determined by using the whole set of data, when applied in each of the 29 weather stations of Fig. 1 (case 1 in Table II). We compared with the accuracy of the formulae that we determined by using only data from the respective weather stations (case 2 in Table II). All the four indicators recognize the fact that, generally, the regression formulas obtained in case 2 are more accurate. However, some non-concordances were observed when we analysed a few particular situations.

Table I. The accuracy of the Equation (2) when applied in Valahia, Moldavia and Ardeal. $m_{CS_{\text{obs}}}$ — the mean of the observed values of cloud shade. MBE — mean bias error, S_D — second centred moment of error distribution, MAE — mean absolute error, d_2 — Willmott's index of agreement (Equation (7)).

	Valahia	Moldavia	Ardeal
$m_{CS_{\text{obs}}}$	0.5479	0.5812	0.5798
MBE	-0.001	-0.001	-0.001
S_D	0.0706	0.0691	0.0671
MAE	0.056	0.053	0.053
d_2	0.9510	0.9433	0.9515

Table II. The accuracy of Equation (2) when applied in different weather stations. Case 1 — regression coefficients determined by using the whole set of data. Case 2 — regression coefficients determined by using only data from the respective weather station. For MBE , S_D , MAE and d_2 see Table I.

Location	MBE		S_D		MAE		d_2	
	Case 1	Case 2						
Botosani	-0.018	-0.001	0.048	0.048	0.041	0.038	0.973	0.976
Suceava	0.019	-0.000	0.057	0.056	0.047	0.042	0.941	0.949
Cotnari	-0.036	-0.000	0.048	0.048	0.048	0.037	0.959	0.973
Iasi	0.038	-0.000	0.069	0.069	0.062	0.053	0.925	0.945
Bacau	-0.008	-0.000	0.043	0.043	0.033	0.032	0.975	0.976
Vaslui	-0.002	-0.001	0.057	0.056	0.043	0.042	0.967	0.970
Birlad	0.092	-0.001	0.081	0.073	0.099	0.068	0.855	0.940
Pt Neamt	0.017	-0.000	0.062	0.062	0.051	0.050	0.928	0.931
Tecuci	-0.037	-0.001	0.042	0.043	0.047	0.034	0.970	0.982
Tg Jiu	-0.042	-0.000	0.079	0.079	0.067	0.065	0.915	0.933
Craiova	0.013	-0.000	0.072	0.070	0.059	0.057	0.957	0.963
Caracal	-0.032	-0.000	0.063	0.062	0.059	0.050	0.955	0.968
Rm Vilcea	-0.021	-0.000	0.060	0.060	0.049	0.048	0.951	0.956
Pitesti	-0.016	-0.000	0.056	0.055	0.046	0.043	0.960	0.967
Tirgoviste	0.037	-0.000	0.071	0.070	0.068	0.056	0.908	0.933
Ploiesti	-0.003	-0.001	0.057	0.057	0.045	0.045	0.966	0.966
Cl Muscel	-0.034	-0.000	0.046	0.043	0.047	0.035	0.940	0.960
Bucarest	0.034	-0.000	0.081	0.079	0.072	0.065	0.930	0.947
Buzau	0.020	-0.001	0.062	0.062	0.053	0.050	0.956	0.961
Constanta	-0.007	-0.000	0.048	0.048	0.039	0.038	0.983	0.984
Sulina	-0.055	-0.003	0.070	0.070	0.072	0.071	0.056	0.963
Satu Mare	0.025	-0.001	0.065	0.064	0.055	0.051	0.947	0.957
Baia Mare	0.015	-0.000	0.065	0.065	0.055	0.052	0.951	0.957
Oradea	0.001	-0.001	0.081	0.071	0.066	0.066	0.930	0.929
Cluj	-0.021	-0.001	0.054	0.053	0.047	0.044	0.964	0.971
Arad	-0.017	-0.000	0.066	0.065	0.056	0.052	0.949	0.959
Timisoara	0.003	-0.001	0.066	0.065	0.053	0.052	0.957	0.959
Deva	0.000	-0.000	0.072	0.072	0.057	0.057	0.941	0.940
Brasov	0.008	-0.001	0.055	0.055	0.042	0.043	0.955	0.955

So, for both cases 1 and 2, the indicators MBE , S_D and MAE show the Equation (2) as having the best performance at Bacau. On the other hand, the index of agreement d estimated the best results at Constanta. The four indicators are in good concordance, showing Birlad as the weather station with the worst results when case 1 is considered. However, in case 2 the index of agreement changes its estimate, showing Piatra Neamt.

A last question that we studied regards the accuracy of Equation (2) when applied in other time-periods than the one when the regression coefficients were determined. First, the empirical relationship obtained by using the whole set of data was applied during six different years (Table III, case 1). The results were compared with those obtained with the regression formulae determined by using only data from the respective years (case 2 of Table III). As expected, the best results were obtained in the case 2. In both cases 1 and 2 the indicators MBE , S_D and MAE show Equation (2) to have the best and the worst performances in the years 1969 and 1968, respectively. Note that the index of agreement is always in good concordance with the other indicators. Second, we analysed the accuracy of the formula we obtained by using the complete set of data, when applied in all the year months (case 1 of Table IV). We compared with the accuracy of the formulas that we determined by using only data from the respective months (Table IV, case 2).

Generally, the index of agreement is in good concordance with the other indicators showing the best results were obtained in case 2. However, note that d_2 , S_D and MAE disagree concerning the months with the best and the worst results, respectively.

5. Conclusion

In this paper we compared the estimations provided by the index of agreement d_2 proposed by Willmott (1982, 1984) with those predicted by other more usual statistical indicators of accuracy. The results we presented were obtained during the validation of a simple formula (Equation (2)) relating cloud shade to point cloudiness. Generally, the index of agreement was found to be in good concordance with other indicators. However, when a finer analysis is considered, some non-concordances were observed. This is not really surprising but a confirmation of the usual perception that no better statistical indicator exists. Consequently, the index of agreement can be used during model validation, together with other statistical indicators.

Acknowledgments

The author thanks Dr C.J. Willmott for the useful information concerning model validation, and also thanks the referee for his valuable remarks and suggestions. Part of this work was performed at the

Table III. The accuracy of Equation (2), when applied in different years. Case 1 — regression coefficients determined by using the whole set of data. Case 2 — regression coefficients determined by using only data from the respective year. For MBE , S_D , MAE and d_2 see Table II.

Year	MBE		S_D		MAE		d_2	
	Case 1	Case 2						
1967	-0.015	-0.000	0.063	0.063	0.051	0.050	0.952	0.954
1968	0.020	-0.000	0.075	0.073	0.060	0.056	0.945	0.955
1969	0.005	-0.001	0.060	0.060	0.047	0.046	0.973	0.974
1970	0.010	-0.001	0.071	0.070	0.056	0.055	0.947	0.949
1971	-0.006	-0.001	0.969	0.069	0.054	0.054	0.947	0.946
1972	-0.003	-0.000	0.072	0.072	0.058	0.058	0.910	0.911

Table IV. The accuracy of the Equation (2) when applied in different months. Case 1 — regression coefficients determined by using the whole set of data. Case 2 — regression coefficients determined by using only data from the respective month. For MBE , S_D , MAE and d_2 see Table I.

Month	MBE		S_D		MAE		d_2	
	Case 1	Case 2						
January	-0.065	0.000	0.052	0.040	0.070	0.032	0.848	0.944
February	-0.019	-0.000	0.051	0.046	0.043	0.037	0.884	0.892
March	0.013	-0.001	0.053	0.048	0.042	0.037	0.930	0.933
April	0.050	0.000	0.058	0.049	0.059	0.038	0.825	0.886
May	0.061	0.000	0.057	0.050	0.067	0.038	0.732	0.822
June	0.049	-0.000	0.060	0.054	0.062	0.043	0.775	0.825
July	0.018	-0.001	0.058	0.048	0.046	0.036	0.871	0.880
August	0.026	-0.000	0.061	0.045	0.050	0.035	0.871	0.903
September	-0.001	-0.000	0.054	0.048	0.043	0.039	0.941	0.942
October	-0.041	-0.001	0.049	0.046	0.053	0.036	0.913	0.945
November	-0.034	-0.000	0.046	0.048	0.049	0.036	0.927	0.948
December	-0.067	-0.000	0.053	0.054	0.071	0.043	0.836	0.939

University of Southampton, UK, with the support of the Commission of the European Communities within the framework of the TEMPUS Scheme (IMG-91-R0-0117).

References

Badescu, V., 1990: Observations concerning the empirical relationship of cloud shade to point cloudiness. *J Appl Meteorol.* **29**, 1358-1360.

Fox, D.G., 1981: Judging air quality model performance. *Bull Am Meteorol Soc.* **62**, 599-609.

—, 1984: Uncertainty in air quality modelling. *Bull Am Meteorol Soc.* **65**, 27-36.

Hanna, S.R., 1989: Confidence limits for air quality model evaluations, as estimated by Bootstrap and Jackknife Resampling Methods. *Atmos Environ.* **23**, 1385-1398.

Harrison, A.W. and Coombes, C.A., 1986: Empirical relationship of cloud shade to point cloudiness (Canada). *Solar Energy.* **37**, 417-421.

IEA, 1984: Handbook of methods of estimating solar radiation, IEA Task V, Subtask B, Norrkoping: Swedish Meteorological and Hydrological Institute.

Lorimer, G.S., 1989: Validation of air pollution dispersion models. *Clear Air (Aust.).* **23**, 82-88.

Preisendorfer, R.W. and Barnett, T.P., 1983: Numerical model reality intercomparison test using small-sample statistics. *Atmos Sci.* **40**, 1884-1896.

Rangarajan, S., Swaminathan, M.S. and Mani, A., 1984: Computation of solar radiation from observations of cloud cover. *Solar Energy.* **32**, 553-558.

Reddy, S.J., 1974: An empirical method for estimating sunshine from total cloud amount. *Solar Energy.* **15**, 281-284.

Ross, D.G. and Fox, D.G., 1991: Evaluation of an air pollution analysis system for complex terrain. *J Appl Meteorol.* **30**, 909-923.

Willmott, C.J., 1981: On the validation of models. *Phys Geogr.* **2**, 184-194.

—, 1982: Some comments on the evaluation of model performance. *Bull Am Meteorol Soc.* **63**, 1309-1313.

—, 1984: On the evaluation of model performance in physical geography, in spatial statistics and models, (Eds: G.L. Gaile and C.J. Willmott), Dordrecht, D. Reidel Publishing Company.

Willmott, C.J., Ackleson, S.G., Davis, R.E., Feddema, J.J., Klink, K.M., Legates, D.R., O'Donnell, J. and Rowe, C.M., 1985: Statistics for evaluation and comparison of models. *J Geophys Res.* **90(C5)**, 8999-9005.

Won, T.K., 1984: Model validation methods. In Handbook of Methods of Estimating Solar Radiation, Swedish Meteorological and Hydrological Institute, Norrkoping.

Zwiers, F.W. and Thiebaux, H.J., 1987: Statistical considerations for climate experiments. Part I: Scalar tests, Part II: Multivariate Tests. *J Clim Appl Meteorol.* **26**, 464-487.

551.506.2(261.26):359:93/99

Forecasting thunderstorms using thermodynamic indices

M. Abdel Wahab

Department of Meteorology, Cairo University
and

M. El-Menshawy
Meteorological Authority, Cairo, Egypt

Summary

A number of verifications were carried out to investigate the performance of thermodynamic indices as thunderstorm predictors. With two added conditions, the probability of predicting thunderstorms using the K index could reach 85%. The vertical profile of static energy or equivalent potential temperature was found to be very useful in the forecast procedure.

1. Introduction

Thunderstorms are mesoscale phenomena whose formation are influenced by meteorological conditions such as humidity and instability; and the interaction between synoptic and mesoscale effects makes the forecasting problem more difficult. Over Egypt, thunderstorms are most frequent during most of the so-called 'cold season' which extends from late Autumn to late Spring. However, climatological analysis of thunderstorm frequency shows that the majority occur at Mersa Matruh and Cairo during November. Early studies of thundery activity over Egypt concluded that thunderstorms occur when the Sudan monsoon low extends to the north. The warm, humid south-east current from the Red sea then interacts with cold air in the rear of low pressure at the eastern part of Mediterranean. This

type of thunderstorm occurs only in spring and Autumn and is more frequent at Cairo; the winter-type thunderstorms occur when depressions travelling along the Mediterranean stay near Cyprus for few days and are more common at Mersa Matruh. The use of thermodynamic indices has been used for a long time to predict these occurrences. But these indices tend to be a local property, and the phenomenon is also a local one. In this paper some indices will be used to predict thunderstorms and the evaluation will also be included. Mersa Matruh (62306) and Cairo (62366) were chosen because they are radiosonde stations, and in this paper 'thunderstorm' means thunder was heard at the station; it may not have rained.

2. Thunderstorms and static stability

Normally a thunderstorm occurs when, in a conditionally unstable atmosphere, a trigger forces boundary layer air up to the level of free convection. Therefore the use of a measure for stability will certainly be helpful in this matter. Baily (1955) introduced the K index

$$K = T_{850} - T_{500} + T_{d850} - (T - T_d)_{700} \quad (1)$$

and cases of $K \geq 20$ should describe favourable conditions. Two years (1981-1983) of twice-daily observations were used (for Cairo and Mersa Matruh). The computations indicated that K is not a sufficient condition. Two more indices were examined:

$$TT = (T_{850} - T_{500}) + (T_{d850} - T_{d500}) \quad (2)$$

$$AA = (T_{850} - T_{500}) - (S_8 + S_7 + S_6 + S_5) \quad (3)$$

where S_i indicates dew-point depression at level i . Equations (2) and (3) were found to give unsatisfactory results, and so we will concentrate on the use of the K index. Recently Andersson *et al.* (1989) used the same index as predictor of summer-time thunderstorms. Our analysis justifies the use of the same pattern. In some cases K was much greater than 20 but there were no storms.

Two additional conditions were found to represent the occurrences.

- (a) $(T - T_d)_{700} \leq 5^\circ\text{C}$, and
- (b) $T_{500} \leq -15^\circ\text{C}$.

In Table I final scores of successful and unsuccessful forecasts are presented. One condition simply means that $K \geq 20$, three conditions means (a) and (b) in addition. Combining the three conditions simply means that $(T + T_d)_{850} > 0$. This will easily identify conditions suitable for thunderstorms. The K index was found to be enough to express the category of the thunder

K value	$\geq 20 \leq 25$	$> 25 \leq 30$	35
Category	isolated	Widespread	Intensive.

Table I. Final score of successful and unsuccessful forecasts.

Station	No. of cases	1 condition	3 conditions
		yes	no
Mersa Matruh	38	30	8
Cairo	14	8	6

Table II. Skill prediction for both stations where P_d is the probability of detection, P_f is the probability of false alarms and P_s is the probability threat score.

Station Criteria	Cairo		M. Matruh	
	one	three	one	three
P_d	57	86	79	96
P_f	43	18	22	2
P_s	40	70	68	71

Some statistics of success for forecasts at the two stations are shown in Table II. For perfect forecast $P_d = P_s = 100$ and $P_f = 0$ (see Andersson *et al.* (1980)). As was mentioned earlier, the K index with two more criteria gives a reasonable estimate for thunder occurrences, but this estimate is not very helpful in so far as it may be able only to predict thunder at a point. We used system of linear equations to predict parameters of the K index for at least 12 hours in advance and therefore thunder activity. T_{850} , T_{700} and T_{500} were predicted using equations of the form

$$T_{hh} = a + b \cdot T_{1000} + c \cdot T_{850} + d \cdot T_{700} + e \cdot T_{500} + f \cdot T_{300}$$

and T_{d850} and T_{d700} from

$$T_{dhh} = a + b \cdot T_{d1000} + c \cdot T_{d850} + d \cdot T_{d700} + e \cdot T_{700} + f \cdot T_{850}.$$

Inspection of days of thunder occurrences proved that some changes were reported at the 700 hPa level, a similar conclusion reached by Pickup (1982) at 500 hPa. This led us to examine the vertical profile of equivalent potential temperature (θ_e) and static energy (E_s), which were calculated by the formulae

$$\theta_e = \theta \exp \left[(3.376/T_L - 0.00254) \times (1 + 0.81 \times 10^{-3} \cdot r) \right]$$

where θ is potential temperature, r is the mixing ratio, and T_L is the absolute temperature at lifting condensation level (Bolton 1980) and

$$E_s = T(k) + 9.8 \times 10^{-3} \cdot z(m) + 2.5r \text{ (g kg}^{-1}\text{)}.$$

The vertical profile of θ_e was calculated and it was noticed that on days of thunder activity its value was smaller at 700 hPa, than in other cases (Fig. 1). It was noticed that a minimum of equivalent temperature < 285 at 700 hPa will definitely be associated with thunderstorms. This simply shows the combined effect of

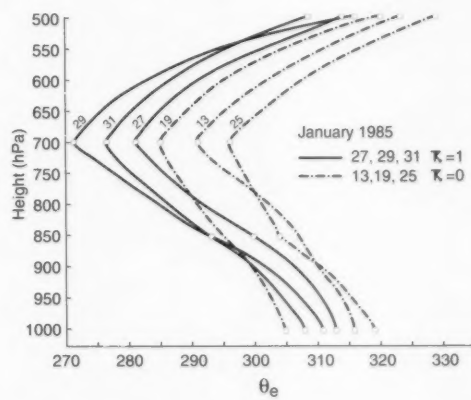


Figure 1. Some cases of stability and instability for equivalent potential temperatures.

temperature and moisture, such potential instability may be released by ascent associated with synoptic-scale motion. Turbulent diffusion of heat and moisture in the vertical act to reduce potential instability, since the net result of the vertical mixing processes is to reduce the vertical gradient of θ_e . The same result has been described other ways in terms of static energy. The solid curve in Fig. 2 show the atmosphere in normal conditions and it need an extra energy of ΔE , to be added on all levels while the minimum static energy still remains at 700 hPa. This index (E_s) was found also to be very successful in describing storm conditions. On the other hand if looking to the boundary force it should also be very valuable in describing storm conditions. This was used by Stone (1984) and Andersson *et al.* (1989) as

$$E = R_d \left| \frac{P_2}{P_1} (T_p - T_e) d \ln p \right|$$

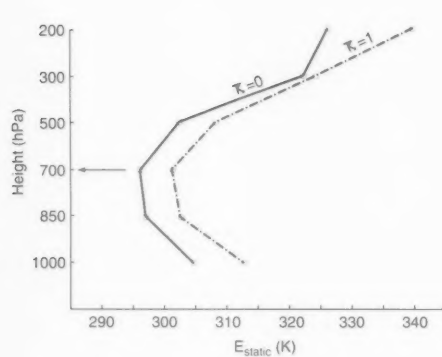


Figure 2. Vertical profile of static energy for two cases with and without thunderstorms.

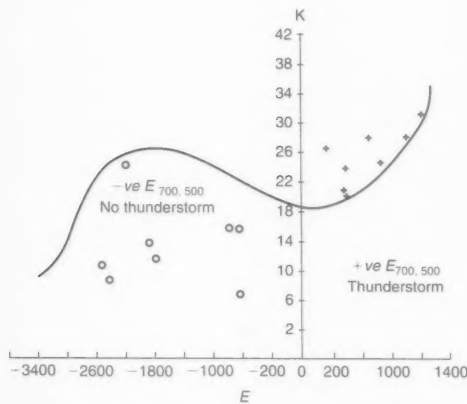


Figure 3. Relationship between E and K index for Cairo.

where P_d is the gas constant for dry air and P_1 and P_2 were taken as 700, 400 hPa respectively and T_p , T_e refer to the parcel and environment temperatures. There are three different cases which can be encountered in the atmosphere, the case when $T_p > T_e$ and therefore E is positive, this makes it possible for vertical motion to develop in the atmosphere usually leading to the formation of convective clouds. In the second where $T_p < T_e$, the energy of instability is negative and upward motion is impossible. Finally, in the case where $T_p > T_e$ at some sub layer and $T_p < T_e$ on another, the overall energy is the algebraic sum of the layers, but usually the cases are too weak to produce thunder. In Fig. 3, a sketch of E and K is given and cases of occurrence are defined, cases were unpicked by K index as in Table I, but reported using the $(E-K)$ combination. A final form using the 4 indices are given in Table III, where skill may reach 90%.

Table III. Combination of different indices using predicted parameters

Station	P_d	Index		
		K	K, θ_e	θ_e, E_s
M. Matruh	P_d	88	91	90
	P_f	15	12	11
	P_s	71	70	73
Cairo	P_d	66	68	72
	P_f	32	27	25
	P_s	54	61	65

3. Conclusion

The main conclusions resulting from this study are as follows (1) The use of the standard K index with two more criteria was found to be a very good indication of thundery activity with skill around 85%. (2) The vertical profile of equivalent potential temperature confirms that a minimum of 285 K or less at 700 hPa is definitely associated with successful prediction if combined with K index. (3) Forecasts of temperature and dew-point temperature will provide a minimum of 12-hour forecast of the phenomenon. (4) Measures of static energy and stability energy may be switched into the forecast procedure, this skill achieved here with a probability of false alarm of about 10%.

References

Andersson T., Andersson, M., Jacobsson, C. and Nilsson, S., 1989: Thermodynamic indices for forecasting thunderstorms in southern Sweden. *Meteorol Mag.*, **118**, 141-146.
 Baily R.E., 1955: Local thunderstorm forecasting. Eastern Airlines Sci. Rep. No.1 to Air Force Geophysics Research Directorate.
 Bolton, D. 1980: On the computations of equivalent potential temperature. *J Atmos Sci.*, **37**, 1816-1820.
 Pickup M.N., 1982: A consideration of the effect of 500 mb cyclonicity on the success of some thunderstorm forecasting techniques. *Meteorol Mag.*, **111**, 87-97.

The publication of the *Meteorological Magazine* will cease with the issue for December 1993.

The December 1993 issue of the *Meteorological Magazine* will be a bumper one of about 40 pages celebrating the Magazine's contribution to the development and dissemination of meteorological knowledge. It will contain a selection of highlights from 1866 up to around 1986.

As one of the leading European establishments for research into meteorology, our publications should be subject to external peer review: this is already the case for much Meteorological Office work. The publication of a new international and European quarterly journal by the Royal Meteorological Society (called *Meteorological Applications*) provides a suitable vehicle for most kinds of articles that have appeared in *Meteorological Magazine*, namely on research, practice, measurements, review articles, applications of meteorology, book reviews, etc. Enquiries should be addressed directly to the Royal Meteorological Society. Non-members should write to:

Journal Subscriptions,
Cambridge University Press,
Edinburgh Building, Shaftesbury Road,
Cambridge CB2 2UV,
United Kingdom

Readers in the USA and Canada should write to:

Journal Subscriptions,
Cambridge University Press,
40, West 20th Street,
New York NY10011,
USA

The United Kingdom Meteorological Office (UKMO) Annual Scientific and Technical Review 1993/94

This Review describes the major developments in science and technology within the UKMO over the year April 1993 to March 1993 and is produced as part of the Meteorological Office Annual Report and became available in July 1994. If you wish to be put on the mailing list for future years please write to:

The News Desk, Publications (room 707a), Meteorological Office, London Road, Bracknell, Berks RG12 2SZ.

Back numbers

Limited stocks of back numbers from 1970 to date are available from:

Vic Silk, The Library, Meteorological Office, London Road, Bracknell, Berks RG12 2SZ; telephone 01344 854074. Copies cost £1.50 each (inclusive). Please send sterling cheques made out to 'Public sub-account HMG 4712'; leave the amount blank but cross them and endorse with the maximum so that the transaction can be made even if some of the requested issues sell out. Please send an addressed label with the order. Remaining stocks will be disposed of in March 1995.

Full-size reprints of Vols 1-75 (1866-1940) are available from Johnson Reprint Co. Ltd., 24-28 Oval Road, London NW1 7DX.

Complete volumes of *Meteorological Magazine* commencing with volume 54 are available on microfilm from University Microfilms International, 18 Bedford Row, London WC1R 4EJ. Information on microfiche issues is available from Kraus Microfiche, Rte 100, Milwood, NY 10546, USA.

November 1993

Edited by R.M. Blackall

Editorial Board: R.J. Allam, N. Wood, W.H. Moores, J. Gloster,
C. Nicholass, G. Lupton, F.R. Hayes

Vol. 122

No. 1456

Contents

	Page
Evaluation of a local climatological model — test carried out in the county of Halland, Sweden. T. Gustavsson and J. Bogren	257
Low-level wind shear at cold fronts. C.P. Pelly	267
A severe hailstorm in northern Greece. S.J. Spanos	270
Polar lows over the North Atlantic. G.C. Craig	278
Infrared imagery showing upper-level waves — 3 May 1993. T.D. Hewson	280
Use of Willmott's index of agreement to the validation of meteorological models. V. Badescu	282
Forecasting thunderstorms using thermodynamic indices. M. Abdel Wahab and M. El-Menshawy	286

ISSN 0026-1149

ISBN 0-11-729348-2



9 780117 293489

